Influence of solution chemistry on the boron content in inorganic calcite grown in artificial seawater

Joji Uchikawa [a,*], Dustin T. Harper [b], Donald E. Penman [c], James C. Zachos [b], Richard E. Zeebe [a]

[a] Department of Oceanography, SOEST, University of Hawaii at Manoa, United States
[b] Department of Earth and Planetary Sciences, University of California, Santa Cruz, United States
[c] Department of Geology and Geophysics, Yale University, United States

Abstract

The ratio of boron to calcium (B/Ca) in marine biogenic carbonates has been proposed as a proxy for properties of seawater carbonate chemistry. Applying this proxy to planktic foraminifera residing in the surface seawater largely in equilibrium with the atmosphere may provide a valuable handle on past atmospheric CO_2 concentrations. However, precise controls on B/Ca in planktic foraminifera remain enigmatic because it has been shown to depend on multiple physicochemical seawater properties. To help establish a firm inorganic basis for interpreting the B/Ca records, we examined the effect of a suite of chemical parameters ($[Ca^{2+}]$, pH, [DIC], salinity and $[PO_4^{3-}]$) on B/Ca in inorganic calcite precipitated in artificial seawater. These parameters were primarily varied individually while keeping all others constant, but we also tested the influence of pH and [DIC] at a constant calcite precipitation rate (R) by concurrent $[Ca^{2+}]$ adjustments. In the simple $[Ca^{2+}]$, pH and [DIC] experiments, both R and B/Ca increased with these parameters. In the pH–$[Ca^{2+}]$ and [DIC]–$[Ca^{2+}]$ experiments at constant R, on the other hand, B/Ca was invariant at different pH and decreased with [DIC], respectively. These patterns agree with the behavior of solution $[B_{Total}/DIC]$ ratio such that, at a fixed $[B_{Total}]$, it is independent of pH but decreases with [DIC]. Based on these results, R and $[B_{Total}/DIC]$ ratio appear to be the primary controls on B/Ca in inorganic calcite, suggesting that both $B(OH)_4^-$ and $B(OH)_3$ are possibly involved in B incorporation. Moreover, B/Ca modestly increased with salinity and $[PO_4^{3-}]$. Inorganic calcite precipitated at higher R and in the presence of oxyanions such as SO_4^{2-} and PO_4^{3-} in growth solutions often undergoes surface roughening due to formation of crystallographic defects, vacancies and, occasionally, amorphous/hydrous $CaCO_3$. These non-lattice sites may provide additional space for B, particularly $B(OH)_3$. Consequently, besides the macroscopic influence of R and bulk solution chemistry, molecular-scale processes associated with calcite nucleation can be an important consideration for B incorporation, especially in complex ionic solutions. Lastly, the covariance of B/Ca with [DIC] and salinity observed here qualitatively agrees with those in planktic foraminifers. It follows that their impact on foraminiferal B/Ca is partly inorganically driven, which may explain why the effect is evident across different species.

1. INTRODUCTION

* Corresponding author at: Dept. of Oceanography, SOEST, Univ. of Hawaii at Manoa, Marine Science Building, 1000 Pope Road, Honolulu, HI 96822, United States.
E-mail address: uchikawa@hawaii.edu (J. Uchikawa).

Marine carbonates ($CaCO_3$) are known to incorporate various elements dissolved in seawater. These elements may occupy non-lattice sites or fully substitute for Ca^{2+}

or CO_3^{2-} positions in the $CaCO_3$ lattice, thereby influencing the fundamental mineral properties such as solubility (Morse and Mackenzie, 1990; Morse et al., 2007). Their incorporation typically depends on the physicochemical state of seawater. Hence, quantification of trace elements in carbonate fossils (e.g., foraminiferal tests) has become an indispensable practice in paleoceanography for probing Earth's geochemical, climatic and environmental history (see reviews by Lea, 1999; Henderson, 2002; Katz et al., 2010).

Boron (B) is one such element that has gained much interest in recent years, despite its low concentrations of ~100 ppm at most in biogenic $CaCO_3$ (Vengosh et al., 1991; Hemming and Hanson, 1992). This stems from the prospect that B abundance in $CaCO_3$ (measured as the B/Ca ratio) could be a useful proxy for ocean carbonate chemistry and, to a greater extent, from the use of B isotopes ($\delta^{11}B$) as a pH proxy. The paleoceanographic utility of these B-based proxies is rooted in the B speciation in seawater and a proposed model of B incorporation into $CaCO_3$. Dissolved B in seawater mainly exists as boric acid $B(OH)_3$ and borate ion $B(OH)_4^-$, and their relative concentration within the total dissolved B ($[B_{Total}] \approx [B(OH)_3]$ $+ [B(OH)_4^-]$) depends on pH (Fig. 1a). Due to a constant isotopic offset, the $\delta^{11}B$ of both $B(OH)_3$ and $B(OH)_4^-$ also

change predictably with pH (Zeebe and Wolf-Gladrow, 2001; Klochko et al., 2006; Foster et al., 2010; Foster and Rae, 2016: see Fig. 1b). Based on broad similarity between the $\delta^{11}B$ of modern marine $CaCO_3$ and that of seawater $B(OH)_4^-$ (Vengosh et al., 1991; Hemming and Hanson, 1992), it was proposed that, as opposed to the neutral $B(OH)_3$, the charged $B(OH)_4^-$ is ultimately substituted with CO_3^{2-} in the $CaCO_3$ lattice (Hemming and Hanson, 1992; Hemming et al., 1995) as follows:

$$CaCO_3 + B(OH)_4^- \rightarrow Ca(HBO_3) + HCO_3^- + H_2O \quad (1)$$

for which a distribution coefficient K_D based on measurable terms (Yu et al., 2007) can be expressed as:

$$K_D = (B/Ca)_{CaCO3}/[B(OH)_4^-/HCO_3^-]_{Solution} \quad (2)$$

Although there are some complications (see a review by Foster and Rae, 2016), a growing number of successive studies, by and large, continue to show reasonable covariance between the $\delta^{11}B$ of $CaCO_3$ of various origins and the $\delta^{11}B$ of $B(OH)_4^-$ and thereby pH (e.g., Henehan et al., 2016; Rae et al., 2011; Hönisch et al., 2004; Reynaud et al., 2004; Trotter et al., 2011; Penman et al., 2013; Farmer et al., 2015, 2016; Sanyal et al., 2000).

Because B abundance in $CaCO_3$ increases with $[B(OH)_4^-]$ (Kitano et al., 1978), a straightforward interpretation of Eq. (1) implies, as is the case for $\delta^{11}B$, B/Ca in $CaCO_3$ should analogously depend on pH due to the interplay between $[B(OH)_4^-]$ and pH (Fig. 1a). Indeed, the pH dependence was confirmed in inorganic calcite (Sanyal et al., 2000; He et al., 2013) and cultured planktic foraminifers (*Orbulina universa*, *Globigerinoides ruber* and *Globigerinoides sacculifer*) (Sanyal et al., 1996; Allen et al., 2011, 2012; Henehan et al., 2015; Holland et al., 2017; Haynes et al., 2017). However, new data from recent inorganic experiments have revealed a more complicated picture. For instance, our research group demonstrated that B/Ca in inorganic calcite increases not only with pH but also with [DIC] (dissolved inorganic carbon, where [DIC] = $[CO_{2(aq)}]$ $+ [HCO_3^-] + [CO_3^{2-}]$) and $[Ca^{2+}]$ (Uchikawa et al., 2015). Elevating pH, [DIC] and $[Ca^{2+}]$ all leads to higher saturation and generally more rapid precipitation. Hence, these results collectively point to kinetic effects associated with calcite precipitation rate (denoted as R), which is consistent with independent experimental results by others (Gabitov et al., 2014; Mavromatis et al., 2015; Kaczmarek et al., 2016). In that study, we additionally grew calcite at two pH values while holding R constant by concurrent $[Ca^{2+}]$ adjustments. The pH dependence was not observed in this case, as the samples yielded virtually identical B/Ca despite the difference in pH (and thus $[B(OH)_4^-]$). This raised a concern that the pH dependence is not necessarily governed by $[B(OH)_4^-]$, thereby challenging our perception of how the B/Ca proxy should work from a theoretical standpoint (Eq. (1)). However, because we used simple $NaCl$–$CaCl_2$– $B(OH)_3$–Na_2CO_3 solutions, whether the results would be directly applicable to calcite precipitated in seawater is still an open question.

We address that issue in this study by performing a new round of calcite precipitation experiments. To close the gap of solution matrix between our experiments and natural
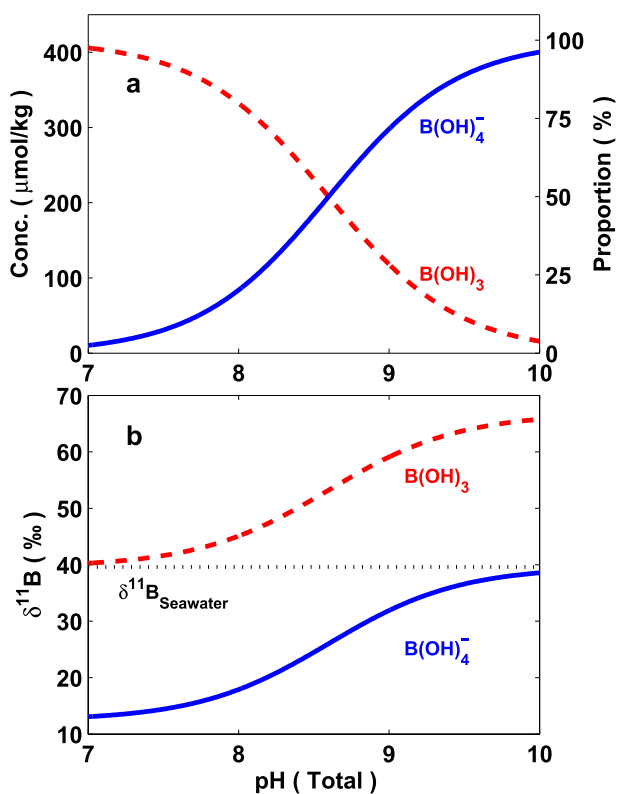

Fig. 1. pH-induced shift in the distribution (Panel a) and isotopic composition (Panel b) of $B(OH)_3$ and $B(OH)_4^-$ at $T = 25\ °C$ and $S = 35$ psu. The system presented here is constrained for modern seawater condition of $[B_{Total}] = 416\ \mu mol/kg$ and $\delta^{11}B_{Seawater} = +39.61‰$ using $pK_B^* = 8.60$ and $^{11-10}\alpha_{B3\text{-}B4} = 1.0272$ (Dickson et al., 2007; Foster et al., 2010; Klochko et al., 2006).

seawater, Mg-free artificial seawater (ASW) was used here. We mainly focused on ground-truthing the influence of pH, [DIC] and [Ca^{2+}] on B/Ca in inorganic calcite grown in ASW. Data from our previous study (Uchikawa et al., 2015) and culture experiments (Allen et al., 2011, 2012; Howes et al., 2017; Holland et al., 2017; Haynes et al., 2017) indicate B/Ca in inorganic and foraminiferal calcite responds quite differently to certain chemical manipulations. One possibility is that, although B/Ca in inorganic calcite is strongly influenced by R (Gabitov et al., 2014; Uchikawa et al., 2015; Mavromatis et al., 2015; Kaczmarek et al., 2016), calcification and/or growth rate may exert a negligible control on foraminiferal B/Ca (Allen et al., 2016; Holland et al., 2017; Haynes et al., 2017). We therefore examined the influence of pH and [DIC] at variable and constant R. Moreover, we took advantage of this opportunity to additionally evaluate the effect of salinity (S) and [PO_4^{3-}]. Allen et al. (2011, 2012) showed that B/Ca in cultured *O. universa*, *G. ruber* and *G. sacculifer* increases with S, while Henehan et al. (2015) recently reported that B/Ca in core-top *G. ruber* co-varies with S, but also with [PO_4^{3-}]. Though still controversial (e.g., Salmon et al., 2016; Quintana Krupinski et al., 2017; Haynes et al., 2017), Henehan et al. (2015) argued that the observed [PO_4^{3-}] effect may be inorganically driven. Our work here marks the first attempt to gauge the influence of S and [PO_4^{3-}] on B/Ca in inorganic calcite.

2. METHODS

2.1. Overview of seeded calcite precipitation experiments

Our experimental approach is fully described in Uchikawa et al. (2015). We grew calcite in a closed isothermal (25 °C) reaction vessel regulated by a titrator system. Once chemical equilibrium was achieved, 80 mg of 10 μm calcite seeds were introduced to initiate calcite overgrowth. Calcite precipitation consumes alkalinity and DIC in a 2:1 molar ratio and concurrently lowers pH as $Ca^{2+} + 2HCO_3^- \rightarrow CaCO_3 + CO_2 + H_2O$ (Zeebe and Wolf-Gladrow, 2001). The titrator system was programmed to dose 0.3 M ^{13}C-spiked Na_2CO_3 solution upon a 0.01 unit of pH decline from assigned values to maintain near-constant B and CO_2 chemistry.

The seeds were rhombohedral in shape and essentially B-free (B/Ca = 1.01 ± 3.30 μmol/mol, ±2σ S.D., $n = 4$), so that B abundance in a given sample (=seeds + overgrowth) was exclusively contributed by the overgrowth fraction. The seeds were also isotopically homogeneous ($\delta^{13}C = -18.6 \pm 0.07‰$, $\delta^{18}O = -21.1 \pm 0.04‰$, VPDB, ±2σ S.D., $n = 5$). By applying a known ^{13}C-spike ($\delta^{13}C_{DIC}$ = +400‰) to the stock Na_2CO_3 solution used for ASW (Section 2.2) and as the titrant, we quantified the fractional abundance of the overgrowth relative to the seeds based on $\delta^{13}C$ mass-balance (see Uchikawa et al., 2015 for details).

We chose the "seeded" precipitation method over other "non-seeded" methods for several reasons. First, the overgrowth tends to inherit the mineralogy of the seeds (Romanek et al., 1992; Zeebe and Sanyal, 2002). This is crucial, given a distinct B compatibility in calcite versus arag-

onite (Kitano et al., 1978; Hemming et al., 1995; Mavromatis et al., 2015). Second, ASW was prepared to a range of calcite saturation that was only sufficient for heterogeneous nucleation onto preexisting nuclei (i.e., the seeds), but not for homogeneous/spontaneous nucleation. Indeed, we observed no precipitation in the absence of seeds. It follows that the onset of precipitation coincided with the timing of seeds addition, which enabled us to determine the experimental duration and R (see Fig. 3 in Uchikawa et al., 2015). This also ensured precipitation in fully stabilized solution chemistry in our experiments, unlike in some other experiments where precipitation may begin freely at any undefined moment while solution chemistry is allowed to drift. Lastly, the seeds provided a reactive surface over which new calcite continued to nucleate. This conceptually resembles the templated shell growth observed in foraminiferal calcification (e.g., Erez, 2003; de Nooijer et al., 2014), which makes our experiments performed in ASW highly relevant for the ongoing effort of establishing reliable calibrations for planktic foraminiferal B/Ca (e.g., Yu et al., 2007; Allen et al., 2011, 2012, 2016; Henehan et al., 2015; Haynes et al., 2017).

To estimate R, we followed the scheme described in Uchikawa et al. (2015). Hereafter, R values are expressed on a logarithmic scale in the unit of mol/m²/s. We assumed that the geometry of the rhombohedral calcite seeds (see Uchikawa et al., 2015) can be approximated to a cubical shape (e.g., Zeebe and Sanyal, 2002) and that calcite precipitation was confined to the seed surface and no homogeneous nucleation occurred. As individual seeds grew in size due to overgrowth, the total surface area changed accordingly over time, which needs to be taken into account for the area-normalized R. For example, the estimates based on the surface area at the beginning and at the end of the experiments reflect the upper and lower limit of R, respectively. We used the total surface area averaged over the entire experimental duration for the area-normalized R, which should be considered as the "time-averaged" precipitation rate. Also, the upper and lower limits were assigned as the error margins for R, as they surpassed the R uncertainty originating from the $\delta^{13}C$ analytical uncertainty.

2.2. Experimental design

We generally followed the recipe of Dickson et al. (2007) for simplified ASW, but excluded $MgCl_2$ addition to avoid aragonite precipitation and the inhibiting effects of Mg^{2+} on calcite precipitation (Morse and Mackenzie, 1990; Morse et al., 2007). The contribution of $MgCl_2$ to the ionic strength was compensated by excess NaCl, which caused relatively high S of ~40 psu in our ASW.

ASW was prepared using N_2-bubbled CO_2-free deionized H_2O as follows. First, NaCl, KCl, Na_2SO_4 and $B(OH)_3$ were dissolved in ~0.8 L of H_2O in a 1 L volumetric flask, to which stock $CaCl_2$ and HCl solution were added. The head-space was flushed with N_2 gas before mixing. In a separate 100 mL flask, Na_2CO_3 solution was prepared to a desired concentration by diluting a stock solution of 0.3 M ^{13}C-spiked Na_2CO_3 under N_2 atmosphere. A small

volume of HCl was also added for pH adjustment. Then, the Na_2CO_3 solution was mixed into the 1 L flask and the final volume was properly adjusted (note that the stock ^{13}C-labaled Na_2CO_3 solution represents the only DIC source for ASW). Finally, ASW was titrated with 0.3 M NaOH (prepared from reagent-grade NaOH and CO_2-free H_2O under N_2 atmosphere) to a desired pH.

In the first set of experiments, pH, [DIC] and [Ca^{2+}] were individually varied. We used NaOH to vary pH. For adjusting [DIC] and [Ca^{2+}], we varied the volume of Na_2CO_3 and $CaCl_2$ solution, respectively, to be added to ASW. In the second set, two of these parameters were varied in pairs (pH–[Ca^{2+}] and [DIC]–[Ca^{2+}] pairs) to maintain near constant R. For example, pH (or [DIC]) was raised while lowering [Ca^{2+}]. The pH–[Ca^{2+}] experiments were performed at a fixed [DIC], and the [DIC]–[Ca^{2+}] experiments were performed at a fixed pH. Even at a constant saturation state, R can vary due to, for example, solution [Ca^{2+}]/[CO_3^{2-}] ratio (Nehrke et al., 2007). The optimum conditions were established in test runs using the titrant addition rate as a crude measure of R. In the third set of experiments, the effects of S and [PO_4^{3-}] were evaluated. We increased/decreased the volume of H_2O to dissolve the constituent salts to modify S. PO_4^{3-} was added to ASW from a stock Na_2HPO_4 solution. We typically performed three replicates for each experimental condition. The data compiled in Table 1 represent the average and $\pm 2\sigma$ S.D. of the results obtained from the replicates, while the individual results are available in the auxiliary material (Table S1).

2.3. Solution chemistry

The pH electrode was calibrated using NBS buffers (at pH 4, 7, 9.18 and 10) due to their range that encompassed our experimental pH range and commercial availability. As described elsewhere (e.g., Zeebe and Wolf-Gladrow, 2001), however, the NBS buffers are inappropriate for measuring samples with high ionic strength such as seawater. Seawater pH is commonly measured on the total scale, for which tris-HCl buffer prepared in synthetic seawater to $S = 35$ psu is used for calibration (Nemzer and Dickson, 2005; Dickson et al., 2007). At $T = 25\,°C$, the reference pH of the tris-HCl buffer on the total scale is 8.0936 (Nemzer and Dickson, 2005). Using our NBS-calibrated electrode, pH of the Dickson-certified tris-HCl buffer was 8.2202 (higher than the reference pH_{Total} value by 0.1266).

We used the CO2SYS program (van Heuven et al., 2009) to constrain the CO_2 chemistry in ASW. Instead of the DOE-recommended stoichiometric dissociation constants (Dickson et al., 2007), we used K_1^*, K_2^*, K_W^*, K_B^* and K_{HSO4-}^* derived from the MyAMI model (Hain et al., 2015) to account for the absence of Mg^{2+} and variable [Ca^{2+}] in our ASW. By default, concentrations of F^-, B_{Total} and SO_4^{2-} are tied to S in the CO2SYS. But [B_{Total}] and [SO_4^{2-}] was not necessarily tied to S in our ASW due to how it was prepared and chemically manipulated. We modified the program to directly load experimental [B_{Total}] and [SO_4^{2-}] and to set [F^-] = 0. These modifications regarding F^- and SO_4^{2-} were important for the conversion of pH

scales by CO2SYS (see Zeebe and Wolf-Gladrow, 2001). We chose pH and [DIC] as the input parameters, because these represent the parameters we directly controlled and because the chemistry of ASW was forced by these parameters. The resulting CO2SYS-derived pH on the total scale was consistently lower than the experimental pH measured on the NBS scale by ∼0.142 units. For our purposes, this is in acceptable agreement with the pH offset of 0.1266 recorded by our pH probe calibrated on the NBS scale (see above). Finally, we followed the algorithm of Zeebe and Wolf-Gladrow (2001) to constrain B chemistry from experimental [B_{Total}], MyAMI K_B^* and the CO2SYS-corrected pH.

2.4. Analytical methods

Calcite samples were analyzed for $\delta^{13}C$ and B/Ca at UC Santa Cruz. Samples were homogenized using a mortar and pestle, and approximately 60 μg and 300 μg were used for $\delta^{13}C$ and B/Ca measurement, respectively.

The $\delta^{13}C$ analyses were performed on a ThermoFinnegan MAT 253 dual-inlet isotope ratio mass spectrometer coupled to a Kiel IV carbonate device. The $\delta^{13}C$ data in Table S1 represent the average and $\pm 2\sigma$ S.D. from duplicate measurements. The $\delta^{13}C$ reproducibility for all samples was $\pm 1.45‰$ on average, which is poorer than the usual measurement reproducibility on natural carbonates ($\pm\sim 0.1‰$). This is likely due to the extreme ^{13}C-labelling applied to our samples ($\delta^{13}C_{Sample} = +\sim 200‰$) relative to the standards, reference gas, and natural samples routinely measured on this instrument (roughly -10 to $+10‰$). However, this should not hamper the overall data quality. As detailed in Uchikawa et al. (2015), with the ^{13}C-spike applied here, $\delta^{13}C$ uncertainty of $\pm 3‰$ would impose an error of 1% in the final estimates for B/Ca in the overgrowth fraction, which is smaller than the analytical precipitation of B/Ca analyses.

The B/Ca analyses were performed on a Thermo Element XR inductively coupled plasma-mass spectrometer following the protocols specifically optimized for our calcite samples (Uchikawa et al., 2015). Calibration was performed by measuring a suite of standards prepared to a range of B/Ca encompassing the B/Ca values measured in this study. All samples were analyzed at [Ca^{2+}] within the range of our standards. We also analyzed a liquid consistency standard once every 5 samples for drift correction. The long-term precision of the B/Ca analyses based on repeat measurements of the consistency standard was better than $\pm 9\%$ or ± 6 μmol/mol ($\pm 2\sigma$ S.D.). Samples were normally analyzed in duplicate. The average B/Ca reproducibility for all samples was ± 7.86 μmol/mol.

3. RESULTS

Titration of ASW by Na_2CO_3 during our experiments counteracted the decline in pH, alkalinity (by providing Na^+) and [DIC] caused by calcite precipitation. It can also be estimated from the $\delta^{13}C$ and B/Ca data that the total B loss was less than 0.02% of the initial [B_{Total}]. Hence, we assume our calcite samples were precipitated under nearly

Table 1
Summary of the experimental conditions and results. Chemical parameters directly manipulated in each experimental series are indicated by bold characters. Calcite precipitation rate R and B/Ca reflect those of the overgrowth fraction in the sample (see text and Uchikawa et al., 2015 for details). All experiments were performed at $T = 25$ °C. The values and accompanying error margins represent the average and $\pm 2\sigma$ S.D. of the results from replicate runs.

Exp. series	Exp.	Replicates n	pH Total	[DIC] μmol/kg	[HCO$_3^-$] μmol/kg	[CO$_3^{2-}$] μmol/kg	[B$_{Total}$] μmol/kg	[B(OH)$_4^-$] μmol/kg	[Ca^{2+}] mmol/kg	[PO$_4^{3-}$] μmol/kg	S psu	$\log_{10}R$ mol/m^2/s	B/Ca μmol/mol
[Ca^{2+}]	Exp. A	3	8.11	2122.2	1961.7	150.2	418.6	95.1	**10.3**	0.0	39.91	−6.28 ± 0.09	77.14 ± 4.32
	Exp. B	3	8.11	2122.4	1950.3	161.8	418.7	95.9	**12.9**	0.0	39.95	−6.09 ± 0.02	109.45 ± 7.23
	Exp. C	3	8.11	2122.4	1937.4	174.6	418.6	97.2	**15.5**	0.0	40.13	−5.98 ± 0.02	130.48 ± 1.63
	Exp. D	3	8.11	2121.7	1922.4	188.9	418.5	98.6	**18.0**	0.0	40.57	−5.91 ± 0.04	148.31 ± 5.37
pH	Exp. A	3	**8.11**	2122.2	1961.5	150.4	418.6	95.1	10.3	0.0	39.96	−6.30 ± 0.02	70.45 ± 4.17
	Exp. B	4	**8.23**	2122.7	1923.1	191.9	418.7	116.2	10.3	0.0	39.74	−5.94 ± 0.08	117.36 ± 10.83
	Exp. C	3	**8.36**	2122.2	1866.1	250.5	418.6	142.6	10.3	0.0	39.74	−5.77 ± 0.06	156.65 ± 11.11
[DIC]	Exp. A	3	8.11	**2122.7**	1962.6	149.8	418.7	95.0	10.3	0.0	39.79	−6.29 ± 0.03	66.65 ± 2.07
	Exp. B	3	8.11	**2547.1**	2355.5	179.2	418.7	94.7	10.3	0.0	39.81	−6.12 ± 0.02	72.37 ± 7.26
	Exp. C	4	8.11	**2866.9**	2652.9	200.0	418.9	94.4	10.3	0.0	39.54	−6.00 ± 0.05	76.29 ± 5.14
pH–[Ca^{2+}]	Exp. A	3	**8.07**	2122.5	1964.0	146.9	418.7	88.4	**12.9**	0.0	40.03	−6.29 ± 0.05	100.62 ± 9.55
	Exp. B	3	**8.11**	2122.2	1961.5	150.5	418.6	95.1	**10.3**	0.0	39.97	−6.29 ± 0.06	76.52 ± 6.48
	Exp. C	4	**8.17**	2123.4	1958.7	155.8	418.8	104.2	**7.8**	0.0	39.49	−6.30 ± 0.07	76.55 ± 9.44
	Exp. D	3	**8.30**	2123.0	1930.7	185.8	418.8	127.2	**5.2**	0.0	39.26	−6.29 ± 0.05	72.30 ± 13.17
[DIC]–[Ca^{2+}]	Exp. A	3	8.11	**2122.4**	1961.8	150.3	418.7	95.1	**10.3**	0.0	39.93	−6.28 ± 0.05	70.08 ± 3.54
	Exp. B	3	8.11	**2548.6**	2375.9	160.2	418.9	93.2	**7.3**	0.0	39.27	−6.30 ± 0.04	43.34 ± 7.27
	Exp. C	2	8.11	**2867.2**	2680.0	173.3	418.9	92.8	**6.0**	0.0	39.44	−6.28 ± 0.04	33.95 ± 10.59
Salinity	Exp. A	3	8.11	2053.0	1904.7	138.2	405.0	90.6	10.0	0.0	**38.60**	−6.34 ± 0.06	75.75 ± 8.72
	Exp. B	2	8.11	2122.7	1962.6	149.8	418.7	95.0	10.3	0.0	**39.84**	−6.24 ± 0.05	97.23 ± 2.87
	Exp. C	2	8.11	2186.8	2015.3	161.0	431.4	98.9	10.6	0.0	**41.02**	−6.20 ± 0.03	111.50 ± 25.26
[PO$_4^{3-}$]	Exp. A	3	8.11	2122.3	1961.7	150.3	418.6	95.1	10.3	**0.0**	39.94	−6.28 ± 0.06	70.02 ± 3.83
	Exp. B	2	8.11	2123.2	1963.5	149.4	418.8	94.9	10.3	**0.5**	39.72	−6.32 ± 0.06	88.54 ± 1.92
	Exp. C	2	8.11	2123.0	1963.0	149.6	418.8	95.0	10.3	**1.0**	39.75	−6.38 ± 0.04	99.64 ± 18.55

constant CO_2 and B chemistry. In contrast, Ca^{2+} was not replenished in our experiments. Based on stoichiometric calculations, Ca^{2+} drawdown was contained within 15% of the initial $[Ca^{2+}]$ (but, for the most part, within ∼9%). Nonetheless, we observed negligible change in the pace of titrant addition over the course of experimental duration, which implies R remained fairly constant during the experiments despite Ca^{2+} drawdown.

When individually varied, elevating $[Ca^{2+}]$, pH and [DIC] all caused both R and B/Ca to increase (Fig. 2). But, in the paired pH–$[Ca^{2+}]$ and [DIC]–$[Ca^{2+}]$ experiments, varying pH or [DIC] was paired with concurrent $[Ca^{2+}]$ adjustments. With this approach, precipitation occurred at nearly identical R at different pH and [DIC] (Fig. 3, a & c). The pH–$[Ca^{2+}]$ experiments were performed at four different pH values. The B/Ca results between pH

8.11 and 8.30 were indistinguishable at ∼75 μmol/mol within the experimental reproducibility. However, the experiments at pH 8.07 (Exp. A: see Table 1) resulted in anomalously higher B/Ca of ∼100 μmol/mol (Fig. 3b). The B/Ca results from the [DIC]–$[Ca^{2+}]$ experiments show a straightforward decreasing trend with [DIC], where B/Ca decreased by ∼40 μmol/mol over the entire [DIC] range (Fig. 3d). Some of the S and $[PO_4^{3-}]$ experiments were only duplicated (other experiments featuring pH, [DIC] and $[Ca^{2+}]$ manipulations were typically triplicated), which resulted in relatively large experimental B/Ca uncertainty (Fig. 4b and d). Still, the current dataset demonstrates notable trends. The effect of S was tested from 38.6 to 41.0 psu. Within this relatively narrow range, there was an almost negligible increase in R, whereas B/Ca increased by ∼40 μmol/mol. In the case of PO_4^{3-} additions up to
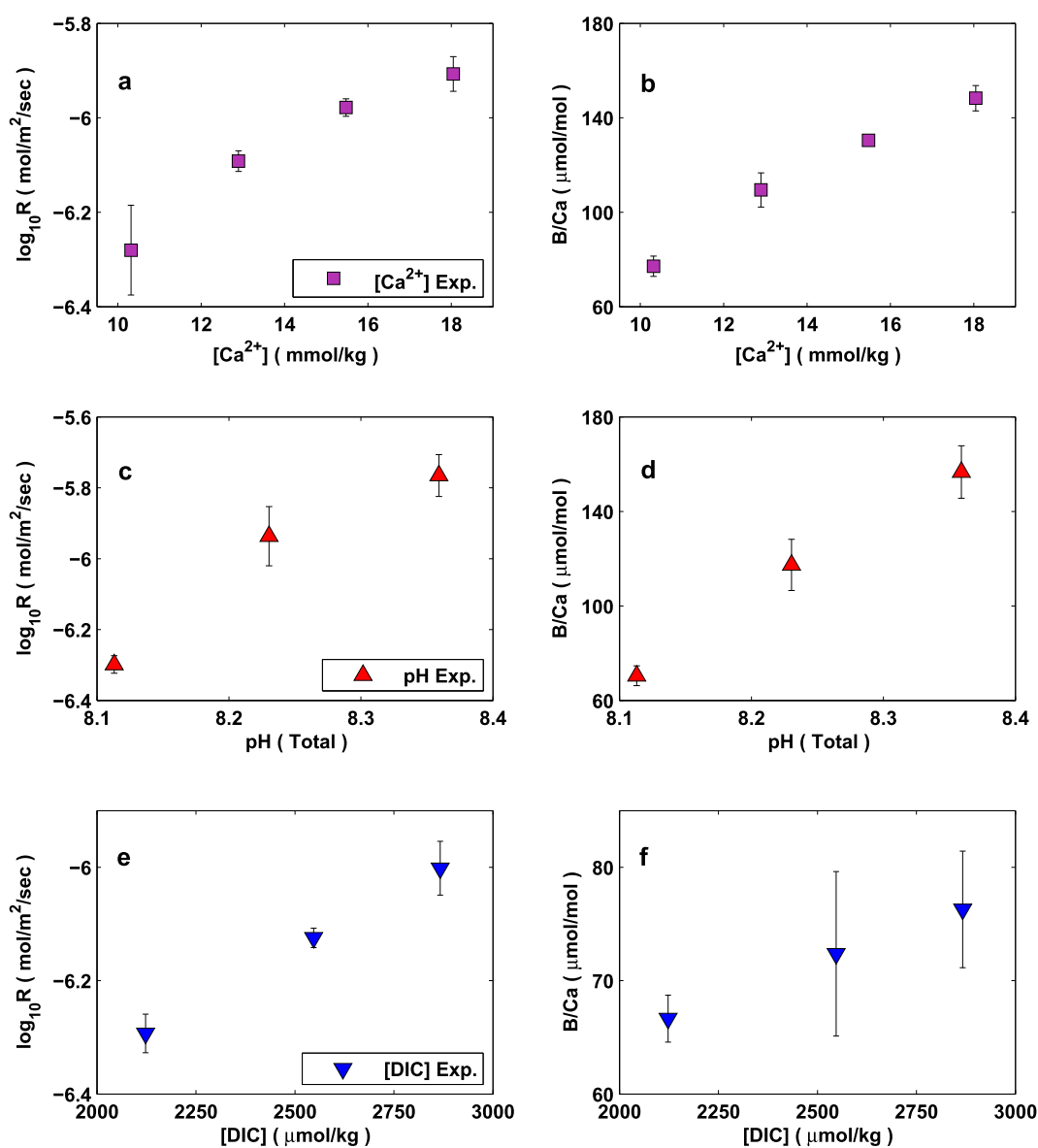

Fig. 2. Impact of the individual manipulations of pH, [DIC] and $[Ca^{2+}]$ on R and B/Ca. In these experiments, only one of the parameters was varied while holding the others constant.
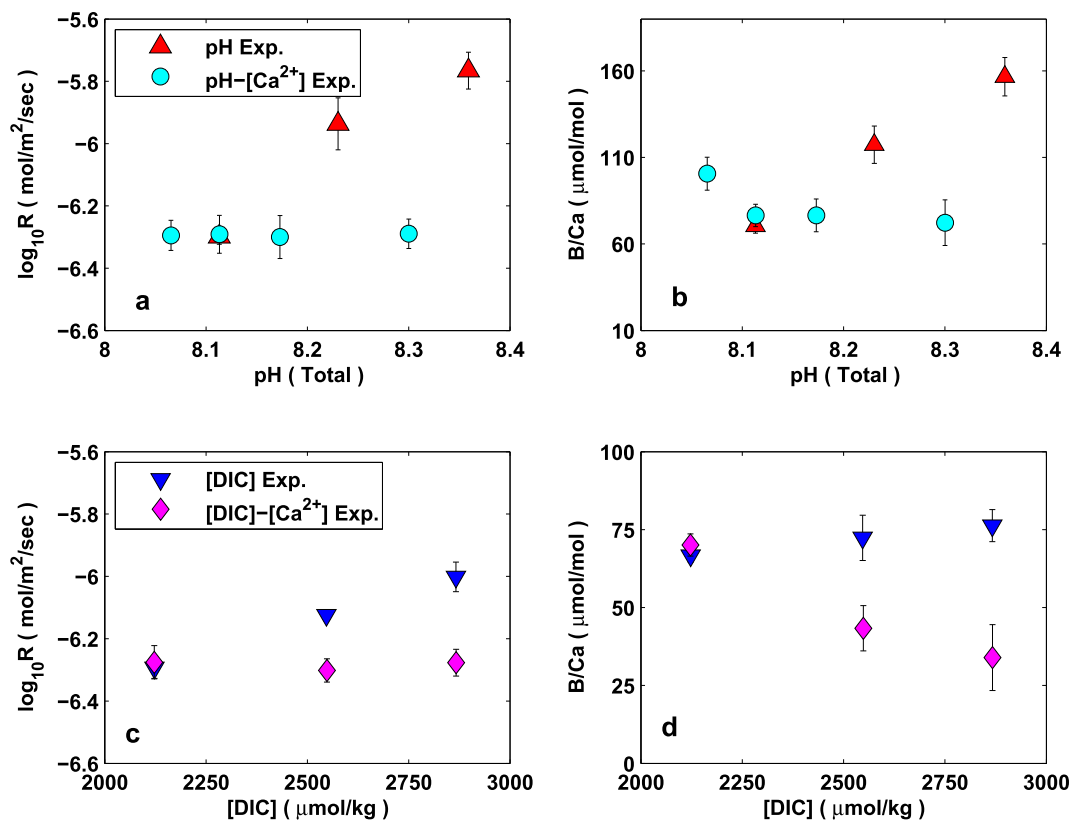
Fig. 3. Comparison of the results from the simple pH and [DIC] experiments (upward and downward triangles, respectively) to those from the paired pH–[Ca^{2+}] and [DIC]–[Ca^{2+}] experiments (circles and diamonds, respectively). For the pH–[Ca^{2+}] experiments, [DIC] was held constant. For the [DIC]–[Ca^{2+}] experiments, pH was held constant.

1 µmol/kg, while R marginally decreased, B/Ca increased by ~30 µmol/mol.

Most of the experiments for the present study was performed at pH and [DIC] reasonably close to Uchikawa et al. (2015), however, [Ca^{2+}] was roughly three times higher in this study. Nevertheless, calcite precipitation generally proceeded at slower rates, for instance, in comparable pH or [DIC] experiments. This presumably reflects a CO$_3^{2-}$ deficit relative to Ca^{2+} (e.g., Nehrke et al., 2007) and/or inhibitions on calcite nucleation caused by various processes in ASW (e.g., ion paring) and on the calcite surface (e.g., kink blocking) due to higher ionic strength and the presence of a more complex mixture of ionic species in ASW. Also, compared to the Uchikawa et al. (2015) experiments performed at [B$_{Total}$] = 432 µmol/kg, calcite samples produced in this study had consistently higher B/Ca at a given R (Fig. 5) despite slightly lower [B$_{Total}$] of ~419 µmol/kg in ASW (except for the S experiments: Table 1).

4. DISCUSSION

4.1. [Ca^{2+}] results and kinetic effects on B/Ca

In response to a roughly 80% increase in [Ca^{2+}] from the baseline concentration of ~10 mmol/kg, R increased from −6.28 to −5.91 (Fig. 2a). This is not as extensive as the

changes in R due to pH manipulations (Fig. 2c). Calcite precipitation proceeds as Ca^{2+} and CO$_3^{2-}$ alternatingly attach to growth kinks to form Ca–CO$_3$ subunits, which eventually coalesce to become a part of the new lattice. Since an equal proportion of Ca^{2+} and CO$_3^{2-}$ is required, the optimum growth condition can be anticipated when they are available in similar abundance (e.g., Nehrke et al., 2007). In the baseline experiment (Exp. A in the [Ca^{2+}] series: Table 1), [Ca^{2+}] was set at the modern seawater concentration of ~10.3 mmol/kg. In contrast, [DIC] was set at 2.1 mmol/kg and CO$_3^{2-}$ accounted for only 7.1% of the total DIC pool at pH 8.11 (i.e., [CO$_3^{2-}$] ≈ 0.15 mmol/kg). Given very high [Ca^{2+}/CO$_3^{2-}$], the bottleneck for calcite nucleation was set by the CO$_3^{2-}$ availability to growth kinks, not by overwhelmingly more abundant Ca^{2+}. This is likely the primary reason why we observed a moderate increase in R in the [Ca^{2+}] experiments.

As shown in Fig. 2b, B/Ca in calcite increased with [Ca^{2+}]. Although other parameters were unaltered, [Ca^{2+}] manipulations automatically influenced the B and DIC speciation due to inherent dependence of the dissociation constants on [Ca^{2+}] (Hain et al., 2015). But these changes are too insignificant to account for the increase in B/Ca with [Ca^{2+}]. The results from the [Ca^{2+}] experiments consequently point to kinetic effects driven by precipitation rate R on B/Ca in inorganic calcite, as we proposed in Uchikawa et al. (2015). Kaczmarek et al. (2016) also
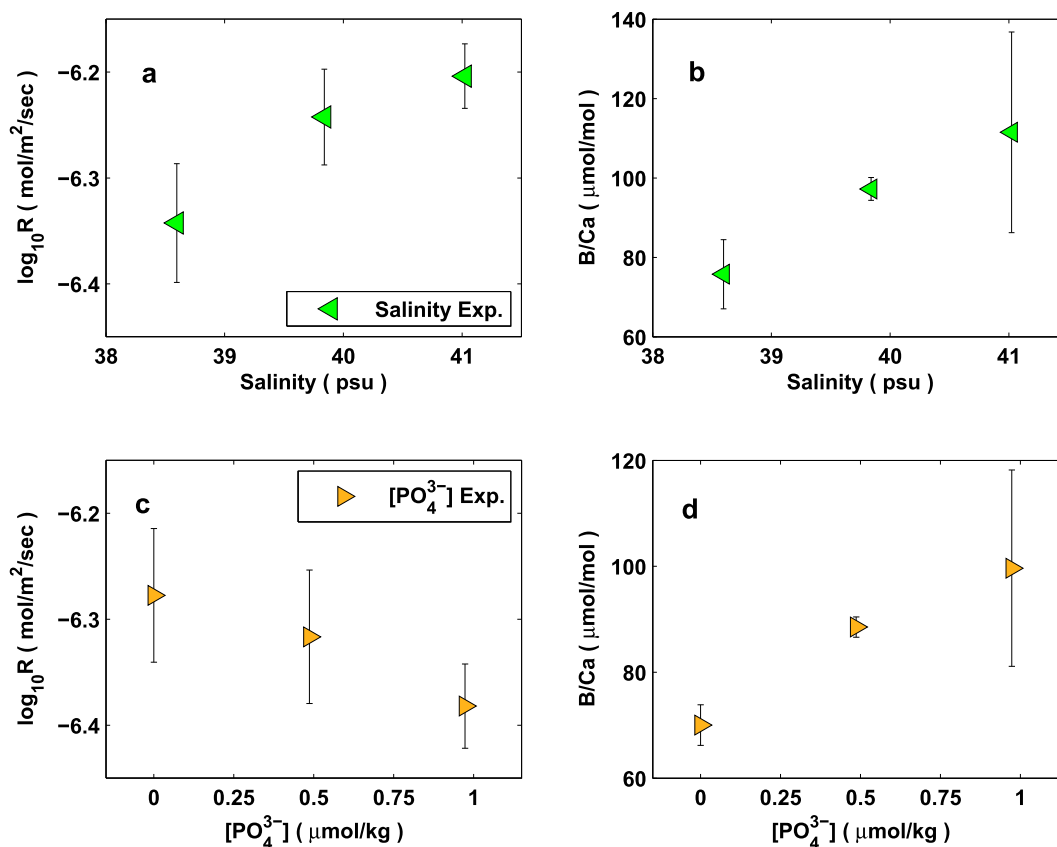
Fig. 4. Summary of the effect of salinity (S) and [PO_4^{3-}] manipulations on R and B/Ca.
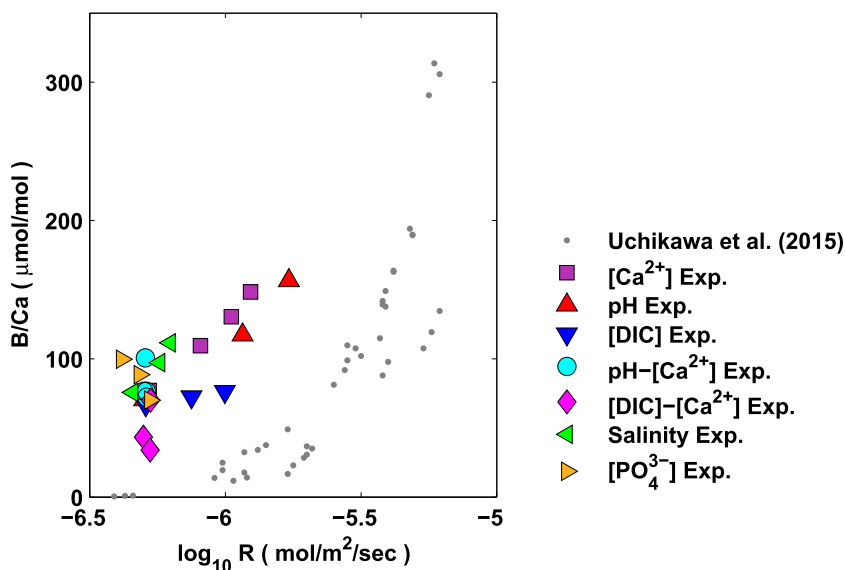

Fig. 5. Comparison of B/Ca as a function of R from Uchikawa et al. (2015) and this study. While fairly simplified and more dilute solutions prepared from NaCl–CaCl$_2$–B(OH)$_3$–Na$_2$CO$_3$ were used in Uchikawa et al. (2015), this study employed Mg-free ASW prepared from NaCl–KCl–Na$_2$SO$_4$–CaCl$_2$–B(OH)$_3$–Na$_2$CO$_3$. The experiments were performed at constant [B$_{Total}$] of ∼419 μmol/kg. For the Uchikawa et al. (2015) data, only the results from the experiments performed at the baseline [B$_{Total}$] of 432 μmol/kg are compiled here. Note that, despite slightly lower [B$_{Total}$], the B/Ca results from this study are consistently higher than those from Uchikawa et al. (2015) at a given R.

applied [Ca^{2+}] manipulations and observed a clear dependence of B/Ca in inorganic calcite on R. Other studies have similarly provided evidence for the dependence of B incorporation on R (Gabitov et al., 2014; Mavromatis et al., 2015). These studies relied on distinct precipitation techniques and growth solutions. Hence, we argue that

kinetic effects on B incorporation is universal in inorganic systems.

4.2. Ground-truthing the pH dependence of B/Ca

We showed in Uchikawa et al. (2015) that, if constant R at different pH can be managed, B/Ca becomes independent of pH. This finding posed a major question to the theoretical ground of the B/Ca proxy (Eq. (1)). However, in fairness, the reliability of these particular results was somewhat compromised by very low total B count in the samples (sample B/Ca below 10 µmol/mol). We circumvented this problem by running our experiments longer to increase the relative contribution of the overgrowth fraction and thus the total B content in the pH–[Ca^{2+}] samples (B/Ca in those samples typically ranged 35–40 µmol/mol).

Broadly speaking, the B/Ca results from the experiments involving pH manipulations display the same trends revealed in Uchikawa et al. (2015). As opposed to the strong pH dependence of B/Ca when R freely co-varied with pH, when R was held constant, B/Ca was indistinguishable between pH 8.11 and 8.30 within the experimental uncertainty (Fig. 3a and b). Since these trends are equally evident in fairly simplified solutions (Uchikawa et al., 2015) and in more complex ASW (this study), they are robust and reproducible irrespective of the difference in the solution matrix. Regardless of whether [Ca^{2+}] was held constant or varied, in both the pH and pH–[Ca^{2+}] experiments, raising pH inevitably caused an increase in [$B(OH)_4^-$] (Table 1). If the pH dependence is ultimately governed by [$B(OH)_4^-$] (Sanyal et al., 2000; He et al., 2013), then we would expect an increase in B/Ca with pH even in the pH–[Ca^{2+}] experiments. But this was clearly not the case. Therefore, our data suggest that the previously recognized pH dependence of B/Ca in inorganic calcite (Sanyal et al., 2000; He et al., 2013) is largely due to kinetic effects associated with R.

An obvious exception to the general agreement between this study and Uchikawa et al. (2015) discussed above is the pH–[Ca^{2+}] experiment at pH 8.07 (Exp. A: see Table 1 and Fig. 3b). In contrast to ~75 µmol/mol of B/Ca for the rest of the pH–[Ca^{2+}] experiments (Exp. B ~ D: Table 1), Exp. A resulted in anomalously higher B/Ca of ~100 µmol/mol. The experiment was triplicated and reproducible (B/Ca = 100.62 ± 9.55 µmol/mol at $R = -6.29 \pm 0.05$, $\pm 2\sigma$ S.D.), which makes it difficult to simply disregard this data point as an outlier. Examining whether or not B/Ca would further increase at lower pH in the pH–[Ca^{2+}] experiments such that the Exp. A data represent a part of a trend ultimately requires additional experiments at lower pH. However, this would be challenging because over 10 mmol of Ca^{2+} is already present in ASW at the baseline condition. Nehrke et al. (2007) observed a substantial decline in calcite growth rate as solution [Ca^{2+}/CO_3^{2-}] ratio progressively deviates from unity in both negative and positive direction. We would predict that our approach to elevate [Ca^{2+}] in order to compensate for a decline in R due to lowering of pH should become more ineffective at lower pH as [Ca^{2+}/CO_3^{2-}] becomes excessively large. We note that Exp. A may be a potentially important observation (e.g.,

Section 4.4), however, in the lack of further confirmation at lower pH, this data will not be discussed further in this paper.

4.3. Competition between DIC and B species

We previously documented that B/Ca increases with [DIC] (Uchikawa et al., 2015). Due to a concurrent increase in R, we argued that the increase in B/Ca with [DIC] largely reflects kinetic effects. In contrast, an opposite trend was revealed in culture studies (Allen et al., 2012; Howes et al., 2017; Holland et al., 2017; Haynes et al., 2017), where B/Ca decreased with [DIC] in both *O. universa* and *G. sacculifer* under similar [DIC] manipulations. This was interpreted by the authors as evidence for competition between B and DIC species during incorporation into $CaCO_3$. This is in line with a recent theoretical study by Balan et al. (2016), who argued that B is fully integrated as the structural component in the calcite lattice in exchange of CO_3^{2-}. If the proposed competition theory is largely an inorganically driven process, it may be likewise in effect during inorganic calcite precipitation. Even so, however, such a signal would be overprinted by kinetic effects if R freely co-varies with [DIC]. To test this, we performed two contrasting [DIC] experiments: the simple [DIC] manipulation experiments at variable R and the paired [DIC]–[Ca^{2+}] experiments at roughly constant R.

Because [DIC] was elevated at a constant pH of 8.17, much of the additional DIC partitioned into the HCO_3^- pool and caused only a fractional increase in [CO_3^{2-}] (Table 1). For that reason, the observed increase in R (from -6.28 to -5.99) with [DIC] was relatively small. Similarly, B/Ca increased only marginally by ~10 µmol/mol. These changes in R and B/Ca are smaller in magnitude compared to the results from the [DIC] experiments of Uchikawa et al. (2015), which reflects the fact that we applied more conservative [DIC] manipulations here (only up to +35% increase) than previously (up to +100%). Nonetheless, we confirmed the positive correlations of both R and B/Ca with [DIC]. In the [DIC]–[Ca^{2+}] experiments, we applied the same levels of [DIC] manipulations (+20% and +35%) but concurrently reduced [Ca^{2+}] to hold R constant in order to eliminate kinetic effects (Fig. 3c, diamonds). In this case, B/Ca systematically decreased with an increase in [DIC] (Fig. 3d, diamonds), in agreement with cultured planktic foraminifers (Allen et al., 2012; Howes et al., 2017; Holland et al., 2017; Haynes et al., 2017). These results support the competition between B and DIC species during incorporation into calcite.

4.4. Synthesis of the [Ca^{2+}], pH and [DIC] results and the primary controls on B/Ca in inorganic calcite

In this study, B/Ca in inorganic calcite increased with [Ca^{2+}], pH and [DIC], when these parameters were individually increased. Importantly, these B/Ca increases were accompanied by concomitant increase in R. More critically, if calcite was forced to precipitate at constant R at different pH and [DIC], B/Ca no longer increased with these parameters (Fig. 3). These results are consistent with Uchikawa et al. (2015), where we highlighted the importance of kinetic
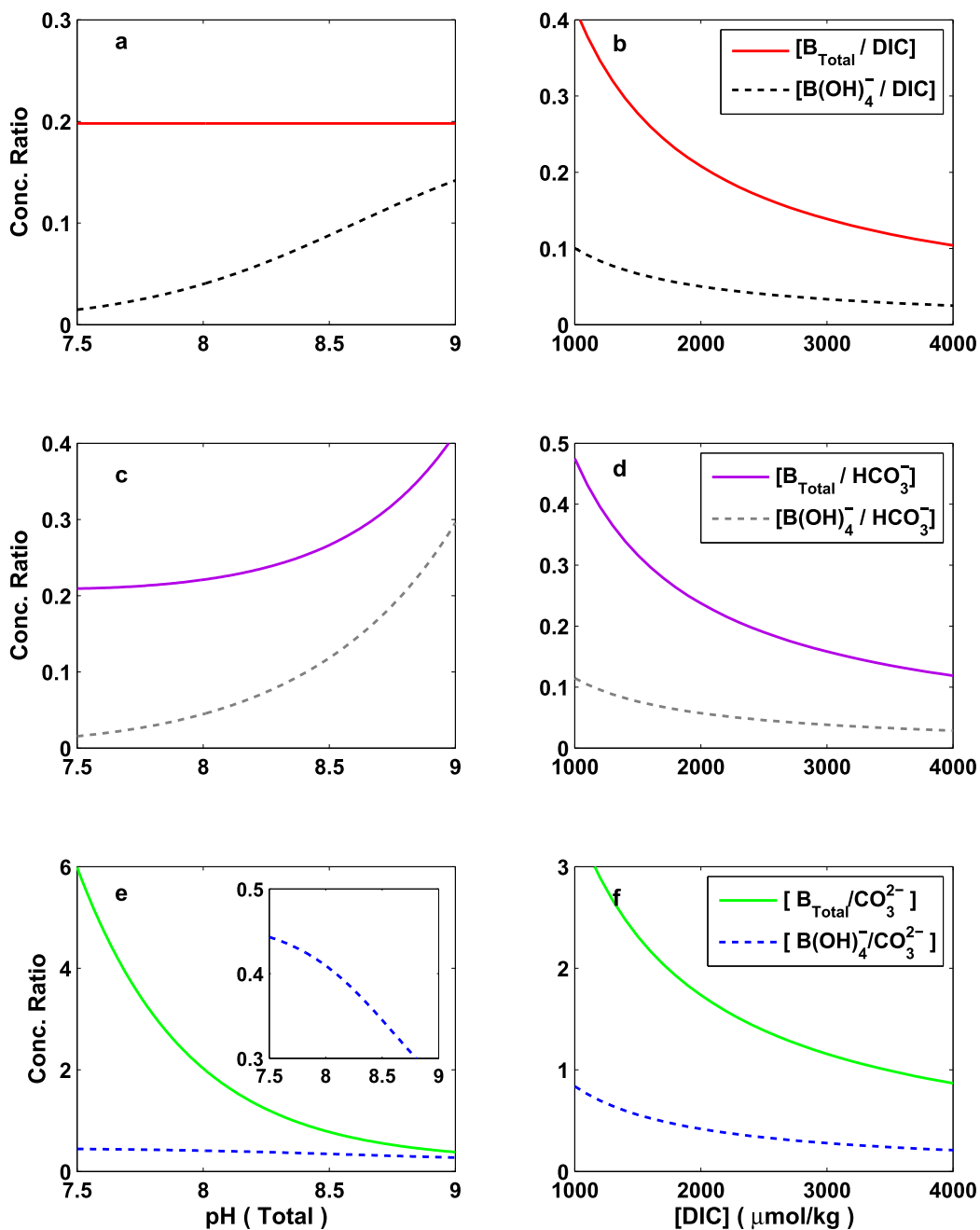
Fig. 6. Comparison of concentration ratios as a function of pH at a constant [DIC] (Panels a, c & e) and as a function of [DIC] at a constant pH (Panels b, d & f) at a fixed [B_{Total}]. (Panels a & b) [B_{Total}/DIC] versus [$B(OH)_4^-$/DIC]. (Panels c & d) [B_{Total}/HCO_3^-] versus [$B(OH)_4^-$/HCO_3^-]. (Panels e & f) [B_{Total}/CO_3^{2-}] versus [$B(OH)_4^-$/CO_3^{2-}]. Note that, [B_{Total}/DIC] remains constant at different pH (Panel a. solid red line), whereas [$B(OH)_4^-$/CO_3^{2-}] actually decreases with pH as clearly shown in the inset (Panel e: dashed blue curve). The CO_2 and B chemistry shown here are calculated from the DOE-recommended constants (Dickson et al., 2007) using the algorithm of Zeebe and Wolf-Gladrow (2001) for the modern seawater [B_{Total}] of 416 µmol/kg. We arbitrarily set [DIC] = 2100 µmol/kg (Panels a, c and e) and pH = 8.1 (Panels b, d and f). (For interpretation of the references to colour in this figure legend, the reader is referred to the web version of this article.)

effects associated with R on B incorporation. Also, given additional experimental evidence (Gabitov et al., 2014; Mavromatis et al., 2015; Kaczmarek et al., 2016), it is undeniable at this stage that R imposes a major control on B/Ca in inorganic calcite.

It is also clear that B/Ca variability cannot be comprehensively explained by R alone (Fig. 5), which suggests there must be additional chemical controls. Hemming and colleagues originally proposed substitutions of CO_3^{2-} in the calcite lattice by $B(OH)_4^-$ (Eq. (1)), for which the distri-

bution coefficient K_D (Eq. (2)) was defined. This expression points to $[B(OH)_4^-/HCO_3^-]$ as the key chemical control. This is consistent with the positive correlation between B/Ca of cultured planktic foraminifers and seawater $[B(OH)_4^-/HCO_3^-]$ (Allen et al., 2011, 2012; Henehan et al., 2015; Howes et al., 2017; Holland et al., 2017; Haynes et al., 2017). Due to the dominance of HCO_3^- in the total DIC pool, however, a covariance between B/Ca and $[B(OH)_4^-/DIC]$ was also evident in those culture data. If $[B_{Total}]$ is fixed, both ratios decrease with [DIC] at a constant pH yet increase with pH at a constant [DIC] (Fig. 6a–d). In our $[DIC]–[Ca^{2+}]$ experiments, we observed a decrease in B/Ca with [DIC] (Fig. 3d, diamonds). This is *compatible* with $[B(OH)_4^-/HCO_3^-]$ and/or $[B(OH)_4^-/DIC]$ being the primary control. But in the pH–$[Ca^{2+}]$ experiments, B/Ca was independent of pH (Fig. 3b, circles, but ignoring Exp. A at pH 8.07: see Section 4.2). This is *not compatible* with either of the above ratios being the primary chemical control. On the contrary, $[B_{Total}]/[DIC]$ decreases with [DIC] at a fixed pH but remains constant with an increase in pH (Fig. 6a and b), which are consistent with our results from both the pH–$[Ca^{2+}]$ and $[DIC]–[Ca^{2+}]$ experiments. Hence, as we initially proposed in Uchikawa et al. (2015), R and $[B_{Total}/DIC]$ appear to be the primary controls on B/Ca in inorganic calcite. The latter parameter implies that B incorporation into calcite involves not only $B(OH)_4^-$ but also $B(OH)_3$.

Meanwhile, Holcomb et al. (2016) argued $[B(OH)_4^-]$ and $[CO_3^{2-}]$ are crucial for B/Ca in inorganic aragonite. In Uchikawa et al. (2015), we did not explicitly consider CO_3^{2-} (i.e., $[B(OH)_4^-/CO_3^{2-}]$ versus $[B_{Total}/CO_3^{2-}]$) mainly because the CO_3^{2-} contribution in the total DIC pool was fairly small (below 10%) for most of the experiments. But Holcomb et al. (2016) pointed out that $[B(OH)_4^-/CO_3^{2-}]$ is as equally effective as $[B_{Total}/DIC]$ in explaining the B/Ca variability against R in the data presented in Uchikawa et al. (2015) ($r^2 = 0.8851$ versus 0.8885, respectively). While it is difficult to decide if exponential (e.g., Uchikawa et al., 2015) or linear fit would be appropriate due to relatively narrow R range for the new data presented here, $[B(OH)_4^-/CO_3^{2-}]$ and $[B_{Total}/DIC]$ again appear to be equally strong in explaining the B/Ca variability (Fig. 7d and e). Yet, at a fixed $[B_{Total}]$, $[B(OH)_4^-/CO_3^{2-}]$ decreases with both [DIC] (at a constant pH) and pH (at a constant [DIC]) as shown in Fig. 6e and f. The latter trend disagrees with the results from the pH–$[Ca^{2+}]$ experiments (Fig. 3b, circles), where B/Ca was invariant at different pH values (although Exp. A at pH 8.07 may be an important consideration if it can be further validated: see Section 4.2). Moreover, $\delta^{11}B$ values of the samples from the pH variation experiments performed in Uchikawa et al. (2015) were higher than $\delta^{11}B$ of $B(OH)_4^-$ by at least $\sim$4‰ (Farmer et al., 2016). Independent experimental data by others (Sanyal et al., 2000; Noireaux et al., 2015) similarly show a few ‰ of ^{11}B enrichment in inorganic calcite relative to $B(OH)_4^-$ (see Fig. 3 in Farmer et al., 2016). Although this is a controversial subject and other processes could be certainly responsible (see a review by Foster and Rae, 2016), these $\delta^{11}B$ data are in line with the possibility of $B(OH)_3$ contribution in addition to $B(OH)_4^-$. In summary, the combination of our direct experimental evidence (the pH–$[Ca^{2+}]$ and $[DIC]–[Ca^{2+}]$ results: see Figs. 3 and 6) and the lines of discussion presented here provide a support for R and $[B_{Total}/DIC]$ being the primary controls for B/Ca in inorganic calcite, both in simple (Uchikawa et al., 2015) and more complex ionic solutions (this study).

In Uchikawa et al. (2015), we found that the consideration of $[B_{Total}]$ over $[B(OH)_4^-]$ becomes progressively more important in explaining the B/Ca variability at higher R (above $\sim$5.5: see Fig. 9 in Uchikawa et al., 2015). We suggested there that both aqueous $B(OH)_4^-$ and $B(OH)_3$ may come into contact with the calcite surface, however, $B(OH)_4^-$ will be attached more firmly due to its charge (e.g., Hemming and Hanson, 1992). Thus, under slow precipitation, $B(OH)_3$ is likely detached from the surface and only $B(OH)_4^-$ will be incorporated (e.g., Hemming and Hanson, 1992), whereas $B(OH)_3$ may be trapped in the $CaCO_3$ matrix before detachment upon rapid precipitation (e.g., Watson, 2004; DePaolo, 2011). Our new data from this study unfortunately fell short of the R threshold of $\sim$5.5. Nevertheless, the partition coefficients based on $[B_{Total}]$ continue to provide better fits, especially at higher R (Fig. 7). This finding pairs well with a recent theoretical work of Balan et al. (2016), who suggested the possibility of multiple incorporation pathways in calcite. They argued that both $B(OH)_4^-$ and $B(OH)_3$ can be incorporated into the calcite lattice as partly deprotonated trigonal $BO_2(OH)^{2-}$ after proper coordination change and/or deprotonation steps. They further argued that aqueous $B(OH)_3$ may also be directly integrated into non-lattice sites upon rapid precipitation involving the formation of disordered (i.e., hydrous/amorphous) $CaCO_3$. In their classic paper, Hemming et al. (1995) also postulated that B could occupy both the structural sites and crystallographic defects. The abundance of defects and lattice deformation in $CaCO_3$ are known to increase with R, especially in complex ionic solutions (Paquette and Reeder, 1995; Xu et al., 2016; Yoshimura et al., 2017). Hence, this incorporation pathway involving $B(OH)_3$ may be of particular relevance to our experimental data.

4.5. The effect of S and PO_4^{3-} on B/Ca in inorganic calcite

S and $[PO_4^{3-}]$ were varied over a relatively narrow range (38.6–41.0 psu and 0–1 μmol/kg, respectively: Table 1), over which B/Ca roughly increased by 35 μmol/mol with S and by 30 μmol/mol with $[PO_4^{3-}]$ (Fig. 4). To the best of our knowledge, these results provide the first confirmation that the S and $[PO_4^{3-}]$ effect revealed in planktic foraminiferal B/Ca from culture and core-top studies (Allen et al., 2011, 2012; Henehan et al., 2015) likewise influence B/Ca in inorganic calcite. Unlike in the $[Ca^{2+}]$, pH and [DIC] experiments, the increase in B/Ca with S and $[PO_4^{3-}]$ were not accompanied by a robust increase in R (compare Figs. 2 and 4). While R increased only subtly with S, R slightly decreased with $[PO_4^{3-}]$, presumably due to the inhibitory effect of PO_4^{3-} on $CaCO_3$ precipitation (Mucci, 1986; Burton and Walter, 1990; Dove and Hochella, 1993; Lin and Singer, 2006). Therefore, the increase in B/Ca with S and $[PO_4^{3-}]$ cannot be attributed to kinetic effects.
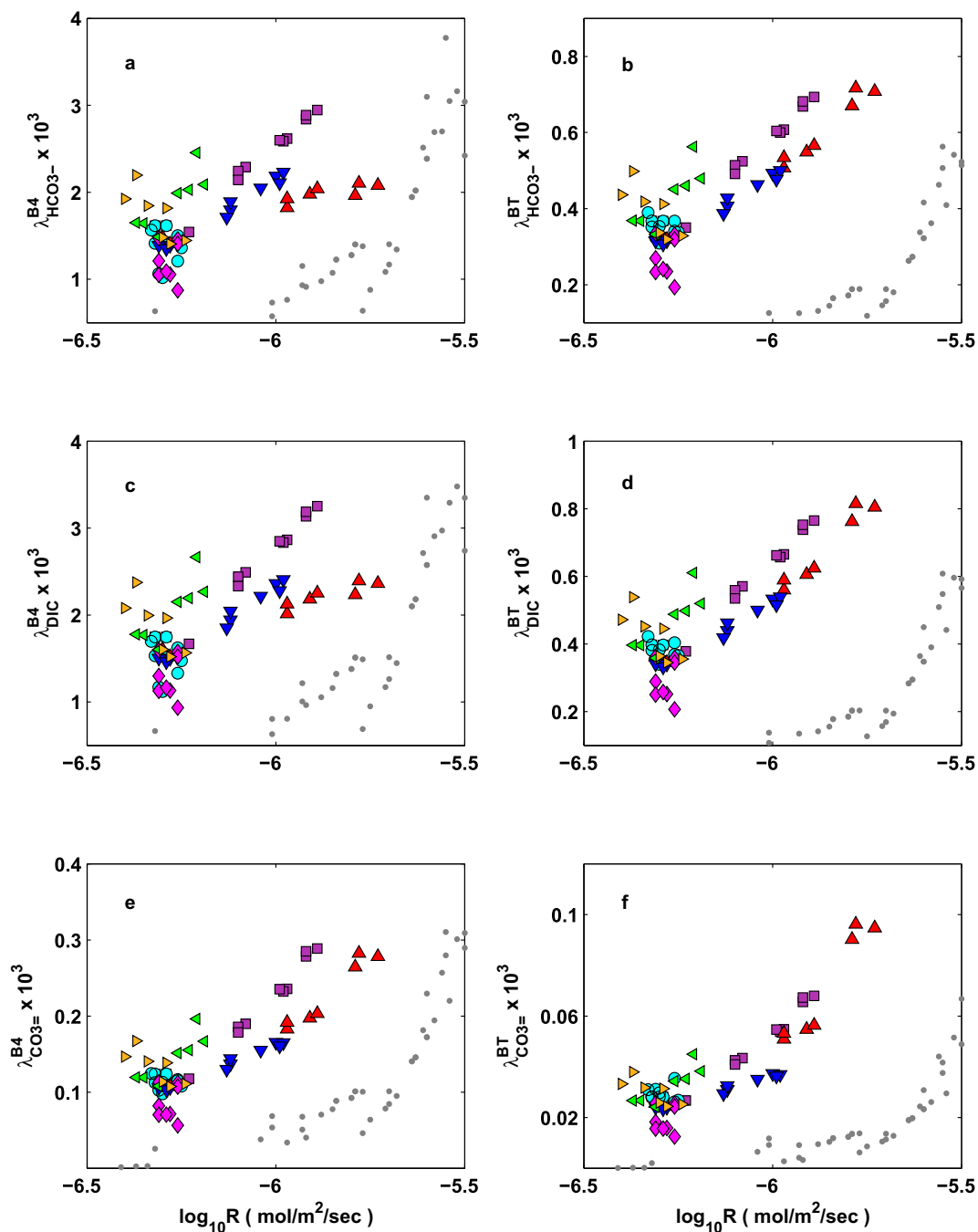
Fig. 7. Comparative assessment of partition coefficients (λ) as a function of R. (Panel a) $\lambda_{HCO3}^{B4} = (B/Ca)/[B(OH)_4^-/HCO_3^-]$, which is same as the distribution coefficient K_D (Eq. (2)). (Panel b) $\lambda_{HCO3-}^{BT} = (B/Ca)/[B_{Total}/HCO_3^-]$. (Panel c) $\lambda_{DIC}^{B4} = (B/Ca)/[B(OH)_4^-/DIC]$. (Panel d) $\lambda_{DIC}^{BT} = (B/Ca)/[B_{Total}/DIC]$. (Panel e) $\lambda_{CO32-}^{B4} = (B/Ca)/[B(OH)_4^-/CO_3^{2-}]$. (Panel f) $\lambda_{CO32-}^{BT} = (B/Ca)/[B_{Total}/CO_3^{2-}]$. For data legend, refer to Fig. 5. Note that data scatter can be significantly reduced if $[B_{Total}]$ is selected over $[B(OH)_4^-]$ in the partition coefficients, which becomes particularly prominent at higher R. This observation is in agreement with Uchikawa et al. (2015). All of the results from replicate experiments are individually presented here (as we did in Fig. 9 in Uchikawa et al., 2015). Also, this figure covers only a portion of the Uchikawa et al. (2015) data to highlight the results from the present study. For the full range of Uchikawa et al. (2015) data, see Fig. S1 in the auxiliary material.

Our approach to raise S inevitably caused $[B_{Total}]$ to increase from 405 to 431.4 µmol/kg (Table 1), which could be the potential driver of the S effect, given the dependence of B/Ca on $[B_{Total}]$ (Hemming et al., 1995; Uchikawa et al., 2015). Although we did not apply direct $[B_{Total}]$ manipula-

tions here, we previously observed ~115 µmol/mol of B/Ca increase per a doubling in $[B_{Total}]$ from the baseline concentration of 432 µmol/kg in Uchikawa et al. (2015), or a B/Ca sensitivity of ~0.27 µmol/mol per 1 µmol/kg of $[B_{Total}]$ increase. Adopting this sensitivity, a 26.4 µmol/kg of

[B_{Total}] increase due to S manipulations would induce only ~7 μmol/mol of B/Ca increase, which is too small compared to the total increase of ~35 μmol/mol (Table 1).

Kitano et al. (1978) showed that adding NaCl to growth solutions enhances B uptake in inorganic calcite. Balan et al. (2016) hence argued that the observed S effect on foraminiferal B/Ca (Allen et al., 2011, 2012; Henehan et al., 2015) may be driven by Na^+. Specifically, they argued that coupled substitution of CO_3^{2-} with $B(OH)_4^-$ and Ca^{2+} with Na^+ could resolve the charge imbalance and facilitate B incorporation (also see Yoshimura et al., 2017). However, note that raising [Na^+] (whether by adding NaCl or increasing S) likely promotes formation of $Na–B(OH)_4^0$ ion complex. If the incorporation takes place via free Na^+ and $B(OH)_4^-$ ions, rather than $Na–B(OH)_4^0$, then the paired substitution scenario described above becomes questionable. Henehan et al. (2015) similarly argued that the positive correlation between core-top *G. ruber* and [PO_4^{3-}] could be aided by the charge compensation mechanism, where two CO_3^{2-} are substituted by a pair of PO_4^{3-} and $B(OH)_4^-$ upon incorporation. In fact, analogous paired substitution into inorganic calcite does occur for trivalent cations (e.g., Schmidt et al., 2008; Hellebrandt et al., 2016. However, feasibility of this scenario again should be sensitive to the exact species/forms through which phosphate is incorporated into $CaCO_3$. For example, if it takes place via HPO_4^{2-} (Burton and Walter, 1990) and/or $Ca–HPO_4^0$ (Lin and Singer, 2006), then phosphate would not necessarily provide charge compensation.

What was common in the S and [PO_4^{3-}] experiments is an increase in SO_4^{2-} and PO_4^{3-} in ASW. Besides their inhibitory effect on $CaCO_3$ nucleation and precipitation, both are known to co-precipitate with calcite by substituting CO_3^{2-} (Busenberg and Plummer, 1985; Vavouraki et al., 2008; Ishikawa and Ichikuni, 1981; Mucci, 1986; Dove and Hochella, 1993; Kontrec et al., 2004). Recall that, in the absence of kinetic effects, an increase in [DIC] suppressed B incorporation in the paired [DIC]–[Ca^{2+}] experiments (Section 4.3 and Fig. 3c and d, diamonds), most likely due to competition between DIC and B species. If SO_4^{2-} and PO_4^{3-} likewise compete with B, without notable kinetic effects (Fig. 4a and c), B/Ca should decrease with S (and hence [SO_4^{2-}]) and [PO_4^{3-}]. But this was not the case (Fig. 4b and d). This observation implies that these anions do not necessarily compete with B during incorporation, presumably due to their specific site preference in the calcite lattice (e.g., Staudt et al., 1994; Hemming et al., 1998). Also note that, there are apparent size differences between SO_4^{2-} and PO_4^{3-} and lattice-forming CO_3^{2-} (Table 2). Accommodating structurally larger SO_4^{2-} and PO_4^{3-} in the calcite matrix creates significant lattice distortion. For instance, Vavouraki et al. (2008) observed a ~1 Å increase in the height of growth steps on the surface of calcite precipitated from SO_4^{2-}-bearing growth solutions relative to those grown in SO_4^{2-}-free solutions. Busenberg and Plummer (1985) also found greater Na^+ uptake in inorganic calcite in the presence of SO_4^{2-} in growth solutions, which was attributed to the defects and/or interstitial sites caused by SO_4^{2-} uptake into calcite. Analogously, the lattice distortion caused by SO_4^{2-} and PO_4^{3-} may provide additional space for

B to occupy. In addition, calcite crystals grown in solutions containing SO_4^{2-} and PO_4^{3-} tend to form rough and irregular surfaces covered with jagged step edges, surface vacancies and disordered $CaCO_3$ (Dove and Hochella, 1993; Kralj et al., 2004; Vavouraki et al., 2008). These surface irregularities could further facilitate B incorporation, especially $B(OH)_3$ that requires no charge compensation (Balan et al., 2016: also see Section 4.4). As opposed to the SO_4^{2-}-free solutions used in Uchikawa et al. (2015), ASW used here contained ~28 mmol of SO_4^{2-}. Hence, the lattice distortion scenario could account for the higher B/Ca in all of the experiments performed in this study relative to those performed in Uchikawa et al. (2015) (Fig. 5). Although more experimental work is clearly needed, we argue that, while [B_{Total}/DIC] and R represent the primary controls, the presence of SO_4^{2-} and other oxyanions (e.g., PO_4^{3-}) may play ancillary roles in influencing B incorporation in inorganic calcite. Besides the bulk solution CO_2 and B chemistry as well as macroscopic R, our new results therefore highlight the potential importance of the molecular-scale crystallographic processes in the fluid-calcite interface for realistic representations of B incorporation in complex ionic solutions like seawater.

4.6. Comparison of the experimental results to planktic foraminiferal B/Ca

In sharp contrast to the apparent dependence of R and B/Ca on [Ca^{2+}] revealed in inorganic calcite (Fig. 2a and b: also see Uchikawa et al., 2015; Kaczmarek et al., 2016), Haynes et al. (2017) found no response to [Ca^{2+}] manipulations in either calcification rates or B/Ca in cultured *O. universa*. In addition, even the pH and [DIC] manipulations performed in the same study resulted in only modest changes in *O. universa* calcification rates. Allen et al. (2016) and Holland et al. (2017) found no clear correlation between calcification rates and B incorporation in cultured *O. universa*, *G. sacculifer* and *Globigerina bulloides* across different chemical manipulations. Moreover, Allen et al. (2016) and Haynes et al. (2017) demonstrated that foraminiferal calcification rates are a few orders of magnitude slower than the typical range of R where kinetic effects impose a strong influence on B/Ca in inorganic calcite (see Fig. 6 in Haynes et al., 2017). These observations from culture studies collectively indicate that foraminifers maintain more or less steady and very slow calcification rates (relative to R revealed in inorganic experiments) even when saturation state of the ambient seawater

Table 2
Comparison of the coordination and size of B species and select anions that can be precipitated as or with calcite. Data shown here are compiled from Greenwood and Earnshaw (1997).

	Coordination	Bond	Length Å
CO_3^{2-}	Planar trigonal	C—O	1.28
$B(OH)_3$	Planar trigonal	B—O	1.37
$B(OH)_4^-$	Tetrahedral	B—O	1.48
SO_4^{2-}	Tetrahedral	S—O	1.47
PO_4^{3-}	Tetrahedral	P—O	1.53

is elevated, and therefore, calcification rates impose negligible controls on foraminiferal B/Ca. However, as caveats, we note that (1) calcification rates reported from culture studies were averaged over several days of experimental duration, so that instantaneous rates during the episodic pulses of intense foraminiferal calcification can be higher and/or more variable (Spero, 1988; Allen et al., 2016) and that (2) calcification/growth rates could still be important for B/Ca in foraminifers *in situ* (e.g., Salmon et al., 2016; Quintana Krupinski et al., 2017).

Under relatively constant R, B/Ca in our inorganic calcite samples decreased with [DIC] (Fig. 3c and d, diamonds) and increased with S (Fig. 4a and b). These trends are qualitatively consistent with the results from culture experiments with *O. universa*, *G. ruber* and *G. sacculifer* (Allen et al., 2011, 2012; Howes et al., 2017; Holland et al., 2017; Haynes et al., 2017). Although the relatively narrow [DIC] range (~2100 to ~2850 μmol/kg) and high S range (38.6–41 psu) tested in this study may hinder direct extrapolation of our results to those from culture experiments, our experimental results suggest that the dependence of foraminiferal B/Ca on [DIC] and S may be inorganically controlled to some extent, which may explain why these effects are evident across different species.

In inorganic calcite, [B_{Total}/DIC] seems to be the primary chemical control on B/Ca, implying that both $B(OH)_4^-$ and $B(OH)_3$ are involved during incorporation (see Section 4.4). Moreover, crystallographic defects that are known to increase at higher R and in the presence of oxyanions such as SO_4^{2-} and PO_4^{3-} could be an important consideration, particularly for $B(OH)_3$. In contrast, B/Ca of cultured planktic foraminifers shows dependence to [$B(OH)_4^-$/HCO_3^-] and/or [$B(OH)_4^-$/DIC] most strongly (Allen et al., 2011, 2012; Henehan et al., 2015; Howes et al., 2017; Holland et al., 2017; Haynes et al., 2017), which suggests negligible $B(OH)_3$ contribution (also see Allen et al., 2011). Then why does $B(OH)_3$ appear to matter in inorganic calcite but not in foraminifers?

One plausible reason is that inorganic calcite is directly affected by the solution chemistry such as saturation state and the presence/concentration of ions/molecules that may influence the nucleation processes, whereas this is perhaps unlikely in foraminifers secreting $CaCO_3$ from internal fluid that is chemically distinct from the ambient seawater. For example, fluid-calcite partitioning of Mg^{2+} and SO_4^{2-} are lower in foraminiferal calcite by several orders of magnitude than in inorganic calcite (e.g., Allen et al., 2016; Mucci, 1986; Paris et al., 2014; Busenberg and Plummer, 1985), hence foraminifers have ways of discriminating these nucleation/precipitation inhibitors that are known to cause significant lattice deformation once situated in calcite (Erez, 2003; de Nooijer et al., 2014). The organic matrix is also thought to play critical roles in maintaining the mineralogical, compositional and architectural integrity of their shells during calcification (Branson et al., 2016; Erez, 2003). And as discussed before, foraminiferal calcification rates tend to be extremely slow relative to typical ranges of R revealed in laboratory experiments (Allen et al., 2016; Holland et al., 2017; Haynes et al., 2017). For these reasons, the occurrence of crystallographic defects in foraminiferal calcite

may be limited. Moreover, as thoroughly discussed in previous B/Ca and $\delta^{11}B$ calibration studies (see a review by Foster and Rae, 2016), the internal pH of foraminifers is often elevated from the ambient pH. Rink et al. (1998) demonstrated that the internal pH of *O. universa* can be elevated up to 8.8 relative to the ambient pH of about 8.3. Over this pH range, the fractional abundance of $B(OH)_3$ decreases from ~66% at pH 8.3 to ~33% at pH 8.9 (Fig. 1a). Such highly controlled calcification possibly leaves $B(OH)_4^-$ as the dominant source of B into foraminiferal calcite.

Lastly, we found B/Ca in inorganic calcite increases with [PO_4^{3-}] (Fig. 4d). This is at least qualitatively consistent with a positive correlation between [PO_4^{3-}] and B/Ca of core-top *G. ruber* reported by Henehan et al. (2015) (Fig. S2). However, the proposed PO_4^{3-} effect on foraminiferal B/Ca is controversial. Recent sediment trap (Salmon et al., 2016) and core-top (Quintana Krupinski et al., 2017) studies provide no robust evidence of the PO_4^{3-} effect in *G. ruber*, *Neogloboquadrina pachyderma* and *G. bulloides*. Furthermore, core-top data by Yu et al. (2013) show that B/Ca of *N. pachyderma* actually decreases with [PO_4^{3-}] (Fig. S2). From a purely inorganic perspective, it is evident from our data that the positive PO_4^{3-} effect on B/Ca in inorganic calcite cannot be attributed to R-driven kinetic effects (Fig. 4c and d). However, although not in accordance with evidence from culture experiments (Allen et al., 2016; Holland et al., 2017; Haynes et al., 2017), field studies suggest potential importance of growth/calcification rates on B/Ca in planktic foraminifers *in situ* (Salmon et al., 2016; Quintana Krupinski et al., 2017). The PO_4^{3-} effect on foraminiferal B/Ca thus could be driven by growth/calcification rates indirectly via greater food consumption (e.g., Henehan et al., 2015) or enhanced symbiont photosynthesis (e.g., Howes et al., 2017; Quintana Krupinski et al., 2017) in nutrient-rich regions. In this regard, future core-top and field assessment should target both symbiotic and asymbiotic species from the same locations. Notably, Allen et al. (2011) and Haynes et al. (2017) cultured *O. universa* at the same location in southern California. While the former study used ambient seawater, the latter used a half-and-half mixture of ambient and nutrient-free synthetic seawater for culturing, such that there should be 50% difference in [PO_4^{3-}] in theory. With no apparent B/Ca offsets between these studies, Haynes et al. (2017) tentatively concluded PO_4^{3-} is unlikely to impose a major control on B/Ca. This argument is inherently based on an assumption of negligible interannual [PO_4^{3-}] variability in the ambient seawater. As cautioned by the authors, these results therefore should not be taken as definitive evidence yet to disprove the PO_4^{3-} effect. Since culture experiments are clearly advantageous in accentuating the isolated effect of a given parameter, experiments applying direct [PO_4^{3-}] manipulations are warranted.

5. CONCLUSIONS

We analyzed B/Ca in inorganic calcite precipitated from Mg-free ASW. When [Ca^{2+}], pH and [DIC] were solely elevated, both R and B/Ca increased with these parameters.

But when R was held constant at different pH and [DIC] by concurrent [Ca^{2+}] adjustments, B/Ca was invariant at different pH and B/Ca decreased with [DIC]. Based on these data in conjunction with the results from previous studies (Uchikawa et al., 2015; Gabitov et al., 2014; Mavromatis et al., 2015; Kaczmarek et al., 2016), it is evident that R-driven kinetic effects are universal in inorganic calcite, irrespective of the precipitation approach and the solution matrix. Moreover, in accordance with Uchikawa et al. (2015), our new data presented here demonstrate that B/Ca in inorganic calcite is primarily controlled by R and [B_{Total}/DIC], with the latter parameter being particularly important at higher R. In addition, we report for the first time that B/Ca increases with S and [PO_4^{3-}]. As R barely increased with S and actually decreased with [PO_4^{3-}], the B/Ca response to these parameters cannot be attributed to kinetic effects. A recent theoretical work of Balan et al. (2016) suggests multiple B incorporation pathways for calcite. While both $B(OH)_4^-$ and $B(OH)_3$ could be substituted into CO_3^{2-} sites in the lattice after coordination change and/or deprotonation, $B(OH)_3$ could be directly integrated into non-lattice sites (crystallographic defects). The data demonstrated here are collectively consistent with this notion, given that crystallographic defects and disordered (hydrous/amorphous) $CaCO_3$ on the calcite surface are more likely at higher R and in the presence of certain oxyanions such as SO_4^{2-} and PO_4^{3-}. Our data further signify the potential importance of crystallographic processes associated with $CaCO_3$ nucleation for B incorporation, especially in complex ionic solutions like seawater. Finally, in the absence of kinetic effects, we observe qualitatively similar B/Ca responses to changes in [DIC], S and [PO_4^{3-}] in inorganic calcite, as observed in planktic foraminifers (though at different sensitivities). We suggest that the effect of at least [DIC] and S on foraminiferal B/Ca could be partly inorganically driven, which explains why different planktic species demonstrate analogous response to these parameters (e.g., Allen et al., 2012).

ACKNOWLEDGEMENTS

AUTHOR CONTRIBUTIONS

JU designed the study, performed laboratory experiments, and led manuscript preparation. DTH and DEP analyzed $\delta^{13}C$ and B/Ca of calcite samples following the protocols implemented by DEP and optimized by DTH. JU, REZ and JCZ acquired funding and/or managed the laboratory where the research was conducted. All authors contributed to the data interpretation and manuscript preparation. SOEST #10234.

APPENDIX A. SUPPLEMENTARY MATERIAL

REFERENCES

Allen K. A., Hönisch B., Eggins S. M., Yu J., Spero H. J. and Elderfield H. (2011) Controls on boron incorporation in cultured tests of the planktic foraminifer *Orbulina universa*. *Earth Planet Sci. Lett.* **345–348**, 203–211.

Allen K. A., Hönisch B., Eggins S. M. and Rosenthal Y. (2012) Environmental controls on B/Ca in calcite tests of the tropical planktic foraminifer species *Globigerinoides ruber* and *Globigerinoides sacculifer*. *Earth Planet Sci. Lett.* **351–352**, 270–280.

Allen K. A., Hönisch B., Eggins S. M., Haynes L. L., Rosenthal Y. and Yu J. (2016) Trace element proxies for surface ocean conditions: a synthesis of culture calibrations with planktic foraminifera. *Geochim. Cosmochim. Acta* **193**, 197–221.

Balan E., Pietrucci F., Gervais C., Blanchard M., Schott J. and Gaillardet J. (2016) First-principles study of boron speciation in calcite and aragonite. *Geochim. Cosmochim. Acta* **193**, 119–131.

Branson O., Bonnin E. A., Perea D. E., Spero H. J., Zhu Z., Winters M., Hönisch B., Russell A. D., Fehrenbacher J. S. and Gagnon A. C. (2016) Nanometer-scale chemistry of a calcite biomineralization template: implications for skeletal composition and nucleation. *Proc. Natl. Acad. Sci. USA* **113**, 12934–12939.

Burton E. A. and Walter L. M. (1990) The role of pH in phosphate inhibition of calcite and aragonite precipitation rates in seawater. *Geochim. Cosmochim. Acta* **54**, 797–808.

Busenberg E. and Plummer L. N. (1985) Kinetic and thermodynamic factors controlling the distribution of SO_4^{2-} and Na^+ in calcites and selected aragonites. *Geochim. Cosmochim. Acta* **49**, 713–725.

de Nooijer L. J., Spero H. J., Erez J., Bijma J. and Reichart G. J. (2014) Biomineralization in perforate foraminifera. *Earth-Sci. Rev.* **135**, 48–58.

DePaolo D. J. (2011) Surface kinetic model for isotopic and trace element fractionation during precipitation of calcite from aqueous solutions. *Geochim. Cosmochim. Acta* **75**, 1039–1056.

Dickson A. G., Sabine C. L., and Christian, J.R. (2007) Guide to best practices for ocean CO2 measurements. PICES Special Publication 3. Sidney, Canada.

Dove P. M. and Hochella, Jr., M. F. (1993) Calcite precipitation mechanisms and inhibition by orthophosphate: in situ observations by scanning force microscopy. *Geochim. Cosmochim. Acta* **57**, 705–714.

Erez J. (2003) The source of ions for biomineralization in foraminifera and their implications for paleoceanographic proxies. *Rev. Mineral. Geochem.* **54**, 115–149.

Farmer J. R., Hönisch B., Robinson L. F. and Hill T. M. (2015) Effects of seawater-pH and biomineralization on the boron isotopic composition of deep-sea bamboo corals. *Geochim. Cosmochim. Acta* **155**, 86–106.

Farmer J. R., Hönisch B. and Uchikawa J. (2016) Single laboratory comparison of MC-ICP-MS and N-TIMS boron isotope analyses in marine carbonates. *Chem. Geol.* **447**, 173–182.

Foster G. L. and Rae J. W. B. (2016) Reconstructing ocean pH with boron isotopes in foraminifera. *Annu. Rev. Earth Planet. Sci.* **44**, 207–237.

Foster G. L., Pogge von Strandmann P. A. E. and Rae J. W. B. (2010) Boron and magnesium isotopic composition of seawater.

Geochem. Geophys. Geosyst. **11**, Q08015. https://doi.org/10.1029/2010GC003201.

Gabitov R. I., Rollion-Bard C., Tripati A. and Sadekov A. (2014) *In situ* study of boron partitioning between calcite and fluid at different crystal growth rates. *Geochim. Cosmochim. Acta* **137**, 81–92.

Greenwood N. N. and Earnshaw A. (1997) *Chemistry of the Elements*, second ed. Butterworth-Heinemann, Oxford.

Hain M. P., Sigman D. M., Higgins J. A. and Haug G. H. (2015) The effects of secular calcium and magnesium concentration changes on the thermodynamics of seawater acid/base chemistry: implications for Eocene and Cretaceous ocean carbon chemistry and buffering. *Global Biogeochem. Cycles* **29**. https://doi.org/10.1002/2014GB004986.

Haynes L. L., Hönisch B., Dyez K. A., Holland K., Rosenthal Y., Fish C. R., Subhas A. V. and Rae J. W. B. (2017) Calibration of the B/Ca proxy in the planktic foraminifer *Orbulina universa* to Paleocene seawater conditions. *Paleoceanography* **32**. https://doi.org/10.1002/2016PA003069.

He M., Xiao Y., Jin Z., Liu W., Ma Y., Zhang Y. and Luo C. (2013) Quantification of boron incorporation into synthetic calcite under controlled pH and temperature conditions using a differential solubility technique. *Chem. Geol.* **337–338**, 67–74.

Hellebrandt S. E., Hofmann S., Jordan N., Barkleit A. and Schmidt M. (2016) Incorporation of Eu(III) into calcite under recrystallization conditions. *Sci. Rep.* **6**, 33137. https://doi.org/10.1038/srep33137.

Hemming N. G. and Hanson G. N. (1992) Boron isotopic composition and concentration in modern marine carbonates. *Geochim. Cosmochim. Acta* **56**, 537–543.

Hemming N. G., Reeder R. J. and Hanson G. N. (1995) Mineral-fluid partitioning and isotopic fractionation of boron in synthetic calcium carbonate. *Geochim. Cosmochim. Acta* **59**, 371–379.

Hemming N. G., Reeder R. J. and Hart S. R. (1998) Growth-step-selective incorporation of boron on the calcite surface. *Geochim. Cosmochim. Acta* **62**, 2915–2922.

Henderson G. M. (2002) New oceanic proxies for paleoclimate. *Earth Planet. Sci. Lett.* **203**, 1–13.

Henehan M. J., Foster G. L., Rae J. W. B., Prentice K. C., Erez J., Bostock H. C., Marshall B. J. and Wilson P. A. (2015) Evaluating the utility of B/Ca ratios in planktic foraminifera as a proxy for the carbonate system: a case study of *Globigerinoides ruber*. *Geochem. Geophys. Geosyst.* **16**. https://doi.org/10.1002/2014GC005514.

Henehan M. J., Goster G. L., Bostock H. C., Greenop R., Marshall B. J. and Wilson P. A. (2016) A new boron isotope-pH calibration for *Orbulina universa*, with implications for understanding and accounting for 'vital effects'. *Earth Planet. Sci. Lett.* **454**, 282–292.

Holland K., Eggins S. M., Hönisch B., Haynes L. L. and Branson O. (2017) Calcification rate and shell chemistry response of the planktic foraminifer *Orbulina universa* to changes in microenvironment seawater carbonate chemistry. *Earth Planet. Sci. Lett.* **464**, 124–134.

Holcomb M., DeCarlo T. M., Gaetani G. A. and McCulloch M. (2016) Factors affecting B/Ca ratios in synthetic aragonite. *Chem. Geol.* **437**, 67–76.

Hönisch B., Hemming G. N., Grottoli A. G., Amat A., Hanson G. N. and Bijma J. (2004) Assessing scleractinian corals as recorders for paleo-pH: empirical calibration and vital effects. *Geochim. Cosmochim. Acta* **68**, 3675–3685.

Howes E. L., Kaczmarek K., Raitzsch M., Mewes A., Bijma N., Horn I., Misra S., Gattuso J.-P. and Bijma J. (2017) Decoupled carbonate chemistry controls on the incorporation of boron into *Orbulina universa*. *Biogeosciences* **14**, 415–430.

Ishikawa M. and Ichikuni M. (1981) Coprecipitation of phosphate with calcite. *Geochem. J.* **15**, 283–288.

Kaczmarek K., Nehrke G., Misra S., Bijma J. and Elderfield H. (2016) Investigating the effects of growth rate and temperature on the B/Ca ratio and δ^{11}B during inorganic calcite formation. *Chem. Geol.* **421**, 81–92.

Katz M. E., Cramer B. S., Franzese A., Hönisch B., Miller K. G., Rosenthal Y. and Wright J. D. (2010) Traditional and emerging geochemical proxies in foraminifera. *J. Foraminiferal Res.* **40**, 165–192.

Kitano Y., Okumura M. and Idogaki M. (1978) Coprecipitation of borate-boron with calcium carbonate. *Geochem. J.* **12**, 183–189.

Klochko K., Kaufman A. J., Yao W., Byrne R. H. and Tossell J. A. (2006) Experimental measurement of boron isotope fractionation seawater. *Earth Planet. Sci. Lett.* **248**, 276–285.

Kontrec J., Kralj D., Brečević L., Falini G., Fermani S., Noethig-Laslo V. and Mirosavljević M. (2004) Incorporation of inorganic anions in calcite. *Eur. J. Inorg. Chem.* **23**, 4579–4585.

Kralj D., Kontrec J., Brečević L., Falini G. and Nöthig-Laslo V. (2004) Effect of inorganic anions on the morphology and structure of magnesium calcite. *Chem. Eur. J.* **10**, 1647–1656.

Lea D. W. (1999) Trace elements in foraminiferal calcite. In: Modern Foraminifera (ed. B. K. Sen Gupta). Kluwer Academic Publishers, Great Britain.

Lin Y.-P. and Singer P. C. (2006) Inhibition of calcite precipitation by orthophosphate: speciation and thermodynamic considerations. *Geochim. Cosmochim. Acta* **70**, 2530–2539.

Mavromatis V., Montouillout V., Noireaux J., Gaillardet J. and Schott J. (2015) Characterization of boron incorporation and speciation in calcite and aragonite from co-precipitation experiments under controlled pH, temperature and precipitation rate. *Geochim. Cosmochim. Acta* **150**, 299–313.

Morse J. W., and Mackenzie F. T. (1990) Geochemistry of Sedimentary Carbonates. (Developments in Sedimentology 48). Elsevier, Amsterdam. 707 pp.

Morse J. W., Arvidson R. S. and Lüttge A. (2007) Calcium carbonate formation and dissolution. *Chem. Rev.* **107**, 342–381.

Mucci A. (1986) Growth kinetics and composition of magnesian calcite overgrowths precipitated from seawater: quantitative influence of orthophosphate ions. *Geochim. Cosmochim. Acta* **50**, 2255–2265.

Nehrke G., Reichart G. J., Van Cappelen P., Meile C. and Bijma J. (2007) Dependence of calcite growth rate and Sr partitioning on solution stoichiometry: non-Kossel crystal growth. *Geochim. Cosmochim. Acta* **71**, 2240–2249.

Nemzer B. V. and Dickson A. G. (2005) The stability and reproducibility of Tris buffers in synthetic seawater. *Mar. Chem.* **96**, 237–242.

Noireaux J., Mavromatis V., Gaillardet J., Schott J., Montouillout V., Louvat P., Rollion-Bard C. and Neuville D. R. (2015) Crystallographic control on the boron isotope paleo-pH proxy. *Earth Planet. Sci. Lett.* **430**, 398–407.

Paquette J. and Reeder D. J. (1995) Relationship between surface structure, growth mechanism, and trace element incorporation in calcite. *Geochim. Cosmochim. Acta* **59**, 735–749.

Paris G., Fehrenbacher J. S., Sessions A. L., Spero H. J. and Adkins J. F. (2014) Experimental determination of carbonate-associated sulfate δ^{34}S in planktonic foraminifera shells. *Geochem. Geophys. Geosyst.* **15**, 1452–1461. https://doi.org/10.1002/2004GC005295.

Penman D. E., Hönisch B., Rasbury E. T., Hemming N. G. and Spero H. J. (2013) Boron, carbon, and oxygen isotopic composition of brachiopod shells: intra-shell variability, controls, and potential as a paleo-pH recorder. *Chem. Geol.* **340**, 32–39.

Quintana Krupinski N. B., Russell A. D., Pak D. K. and Paytan A. (2017) Core-top calibration of B/Ca in Pacific Ocean *Neogloboquadrina incompta* and *Globigerina bulloides* as a surface water carbonate system proxy. *Earth Planet Sci. Lett.* **466**, 139–151.

Rae J. W. B., Foster G. L., Schmidt D. N. and Elliott T. (2011) Boron isotopes and B/Ca in benthic foraminifera: proxies for the deep ocean carbonate system. *Earth Planet. Sci. Lett.* **302**, 403–413.

Reynaud S., Hemming N. G., Juillet-Leclerc and Gattuso JP. (2004) Effect of *p*CO$_2$ and temperature on the boron isotopic composition of the zooxanthellate coral *Acropora* sp.. *Coral Reef* **23**, 539–546.

Rink S., Kühl M., Bijma J. and Spero H. J. (1998) Microsensor studies of photosynthesis and respiration in the symbiotic foraminifer *Orbulina universa*. *Mar. Biol.* **131**, 583–595.

Romanek C. S., Grossman E. L. and Morse J. W. (1992) Carbon isotope fractionation in synthetic aragonite and calcite: effects of temperature and precipitation rate. *Geochim. Cosmochim. Acta* **56**, 419–430.

Salmon K. H., Anand P., Sexton P. F. and Conte M. (2016) Calcification and growth processes in planktonic foraminifera complicate the use of B/Ca and U/Ca as carbonate chemistry proxies. *Earth Planet. Sci. Lett.* **449**, 372–381.

Sanyal A., Hemming N. G., Broecker W. S., Lea D. W., Spero H. J. and Hanson G. N. (1996) Oceanic *p*H control on the boron isotopic composition of foraminifera: evidence from culture experiments. *Paleoceanography* **11**, 513–517. https://doi.org/10.1029/96PA01858.

Sanyal A., Nugent M., Reeder R. J. and Bijma J. (2000) Seawater pH control on the boron isotopic composition of calcite: evidence from inorganic calcite precipitation experiments. *Geochim. Cosmochim. Acta* **64**, 1551–1555.

Schmidt M., Stumpf T., Fernandes M. M., Walther C. and Fanghänel T. (2008) Charge compensation in solid solutions. *Angew. Chem. Int. Ed.* **47**, 5846–5850.

Spero H. J. (1988) Ultrastructural examination of chamber morphogenesis and biomineralization in the planktonic foraminifer *Orbulina universa*. *Mar. Biol.* **99**, 9–20.

Staudt W. J., Reeder R. J. and Schoonen A. A. (1994) Surface structural controls on compositional zoning of SO_4^{2-} and SeO_4^{2-} in synthetic calcite single crystals. *Geochim. Cosmochim. Acta* **58**, 2087–2098.

Trotter J., Montagna P., McCulloch M., Silenzi S., Reynaud S., Mortimer G., Martin S. and Ferrier-Pagès Gattuso., et al. (2011) Quantifying the pH 'vital effect' in the temperate zooxanthellate coral *Cladocora caespitosa*: validation of the boron seawater pH proxy. *Earth Planet. Sci. Lett.* **303**, 163–173.

Uchikawa J., Penman D. E., Zachos J. C. and Zeebe R. E. (2015) Experimental evidence for kinetic effects on B/Ca in synthetic calcite: implications for potential $B(OH)_4^-$ and $B(OH)_3$ incorporation. *Geochim. Cosmochim. Acta* **150**, 171–191.

van Heuven S., Pierrot D., Lewis E., and Wallace D. W. R. (2009) MATLAB Program Developed for CO$_2$ System Calculations. ORNL/CDIAC-105b. Carbon Dioxide Information Analysis Center, Oak Ridge National Laboratory, US Department of Energy, Oak Ridge, TN. <http://cdiac.ornl.gov/oceans/co2r-prt.html>.

Vavouraki A. I., Putnis C. V., Putnis A. and Koutsoukos P. G. (2008) An atomic force microscopy study of the growth of calcite in the presence of sodium sulfate. *Chem. Geol.* **253**, 243–251.

Vengosh A., Kolodny Y., Starinsky A., Chivas A. R. and McCulloch M. T. (1991) Coprecipitation and isotopic fractionation of boron in modern biogenic carbonates. *Geochim. Cosmochim. Acta* **55**, 2901–2910.

Watson E. B. (2004) A conceptual model for near-surface kinetic controls on the trace-element and stable isotope composition of abiogenic calcite crystals. *Geochim. Cosmochim. Acta* **68**, 1473–1488.

Xu J., Wang J., Hong M. and Teng H. H. (2016) Solution-chemistry control of Mg^{2+}-calcite interaction mechanisms: implication for biomineralization. *Am. Min.* **101**, 1104–1112.

Yoshimura T., Tamenori Y., Suzuki A., Kawahata H., Iwasaki N., Hasegawa H., Nguyen L. T., Kuroyanagi A., Yamazaki T., Kuroda J. and Ohkouchi N. (2017) Altervalent substitution of sodium for calcium in biogenic calcite and aragonite. *Geochim. Cosmochim. Acta* **202**, 21–38.

Yu J., Elderfield H., Hönisch B. (2007) B/Ca in planktonic foraminifera as a proxy for surface seawater pH. Paleoceanography, 22, PA2202. http://dx.doi.org/10.1029/2006PA001347.

Yu J., Thornalley D. J. R., Rae J. W. B. and McCave N. I. (2013) Calibration and application of B/Ca, Cd/Ca, and δ^{11}B in *Neogloboquadrina pachyderma* (sinistral) to constrain CO$_2$ uptake in the subpolar North Atlantic during the last deglaciation. *Paleoceanography* **28**, 237–252. https://doi.org/10.1002/palo.20024.

Zeebe R. E. and Wolf-Gladrow D. A. (2001) *CO$_2$ in Seawater: Equilibrium, Kinetics, Isotopes*. Elsevier Oceanography Series, Elsevier, Amsterdam, p. 346.

Zeebe R. E. and Sanyal A. (2002) Comparison of two potential strategies of planktonic foraminifera for house building: Mg^{2+} or H$^+$ removal? *Geochim. Cosmochim. Acta* **66**, 1159–1169.

Associate editor: Claire Rollion-Bard